Hindawi Publishing Corporation
Advances in Condensed Matter Physics
Volume 2016, Article ID 9273702, 26 pages
http://dx.doi.org/10.1155/2016/9273702

Research Article

Ni-Based Ohmic Contacts to *n*-Type 4H-SiC: The Formation Mechanism and Thermal Stability

A. V. Kuchuk,[1,2,3] P. Borowicz,[1,4] M. Wzorek,[1] M. Borysiewicz,[1] R. Ratajczak,[5] K. Golaszewska,[1] E. Kaminska,[1] V. Kladko,[2] and A. Piotrowska[1]

[1]*Institute of Electron Technology, Aleja Lotnikow 32/46, 02-668 Warsaw, Poland*
[2]*V. Lashkaryov Institute of Semiconductor Physics, National Academy of Sciences of Ukraine, Prospekt Nauky 41, Kyiv 03680, Ukraine*
[3]*Institute for Nanoscience and Engineering, University of Arkansas, West Dickson 731, Fayetteville, AR 72701, USA*
[4]*Institute of Physical Chemistry, Polish Academy of Sciences, Ulica Kasprzaka 44/52, 01-224 Warsaw, Poland*
[5]*National Centre for Nuclear Research, Ulica Andrzeja Sołtana 7, 05-400 Otwock, Poland*

Correspondence should be addressed to A. V. Kuchuk; kuchuk@uark.edu

Received 2 November 2015; Revised 2 February 2016; Accepted 8 February 2016

Academic Editor: Jan A. Jung

The fabrication of low-resistance and thermal stable ohmic contacts is important for realization of reliable SiC devices. For the *n*-type SiC, Ni-based metallization is most commonly used for Schottky and ohmic contacts. Many experimental studies have been performed in order to understand the mechanism of ohmic contact formation and different models were proposed to explain the Schottky to ohmic transition for Ni/SiC contacts. In the present review, we summarize the last key results on the matter and post open questions concerning the unclear issues of ohmic contacts to *n*-type SiC. Analysis of the literature data and our own experimental observations have led to the conclusion that the annealing at high temperature leads to the preferential orientation of silicide at the heterointerface (0001)SiC//(013)δ-Ni_2Si. Moreover, we may conclude that only δ-Ni_2Si grains play a key role in determining electrical transport properties at the contact/SiC interface. Finally, we show that the diffusion barriers with free diffusion path microstructure can improve thermal stability of metal-SiC ohmic contacts for high-temperature electronics.

1. Introduction

The increasing demand for electronic devices capable of functioning at high power and frequency levels, under high temperatures, and in harsh environments is one of the most significant issues of modern information society. Moreover, energy problems and environmental concerns due to global warming have generated a need for novel semiconductor devices for active electrical power management in areas, such as energy generation, distribution, and transport where efficiency and high-temperature operations are of the essence. Silicon carbide (SiC), particularly the 4H polytype (4H-SiC), is one of the key candidates for application in such devices, owing to its excellent intrinsic properties, which involve a large bandgap (3.26 eV), high breakdown electric field (3×10^6 Vcm^{-1}), high electron drift velocity (2×10^7 cm s^{-1}), good thermal conductivity (4.9 W cm^{-1} K^{-1}), and chemical inertness [1–3].

In order to take full advantage of the superior SiC properties, several challenges in material processing need to be overcome. One of the most important issues is the quality and reliability of metal/SiC electrical contacts. This is especially true for the ohmic contacts, which are a part of any semiconductor device. The issue of the ohmic contact formation is primarily important because a high potential barrier is inclined to form at the interface between most metals and SiC, which consequently results in low-current driving, slow switching speed, and increased power dissipation. Thus, the fabrication of reliable and low-resistance ohmic contacts to SiC is still one of the most important problems that need addressing. This paper provides a comprehensive and critical assessment of the fundamentals and practice of Ni-silicide

ohmic contacts to n-type 4H-SiC with an emphasis on high-temperature handling capability.

There exist several review articles on contacts to SiC [4–6]; however, in the last few years many new peer-reviewed papers on metal/SiC contacts were published, often containing contradicting results and conclusions, but no consensus has been reached. Therefore, the aim of this work is to present briefly the last key results on the matter and to post open questions concerning the unclear issues of ohmic contacts to n-type SiC.

2. Ohmic Contacts to 4H-n-SiC: State of the Art

For metal contacts to n-type 4H-SiC, the electron affinity (X_s) and work function of the metal (W_m) are the relevant quantities determining the Schottky barrier height $\varphi_B = W_m - X_s$, due to a sufficiently low density of surface states in 4H-SiC (~10^{12} cm^{-2} eV^{-1}). Thus, according to the Schottky theory, the barrier height φ_B of a metal/4H-n-SiC strongly depends on the electron work function W_m of the metals. Indeed, as is shown in Figure 1, the experimental results of metal/4H-n-SiC contacts confirm this model [7–23].

As is well known, a rectifying (Schottky) metal contact to n-type semiconductor is formed when the electron work function of the metal exceeds the electron affinity of the semiconductor ($W_m > X_s$), and the ohmic contact is formed if $W_m \leq X_s$. Since W_m for most metals exceeds the electron affinity X_s of 4H-SiC (see Figure 1), the formation of ohmic contacts to 4H-n-SiC is typically done by the deposition of the same metals as for the Schottky barriers however with subsequent high-temperature annealing. Such rapid thermal annealing (RTA) causes (i) the creation of a tunnel contact, which consists of a thin barrier, obtained by heavy doping of the semiconductor, through which carriers can readily tunnel and (ii) the formation of new compounds which reduces the barrier height and the width of the depletion region at the metal-semiconductor interface. It should be noted that this paper is focused mainly on Si-face 4H-SiC material. However, the SiC surface polarity (Si-face or C-face) and polytypes (3C, 2H, 6H, etc.) are important considerations for ohmic contact formation. The polarity and polytypes can lead to the difference in barrier height and interaction at the metal/SiC interface for the same metallization scheme [24]. Thus, both of them strongly influence the electrical quality of the contact.

On the basis of previous works [26–45], the common processes in the reaction of metals with SiC can be identified as follows: (i) SiC + refractory metals (Ti, Ta, W, etc.) → RTA → carbides (TiC, TaC, WC, etc.) + silicides ($TiSi_x$, $TaSi_x$, WSi_x, etc.) + ternary phases ($TiCSi_x$, $TaCSi_x$, $WCSi_x$, etc.); (ii) SiC + other metals (Ni, Pd, Pt, etc.) → RTA → silicides ($NiSi_x$, $PdSi_x$, $PtSi_x$, etc.) + C.

The fabrication of ohmic contacts to SiC may be achieved using various metallization schemes; and for the n-type SiC, Ni and Ni-based contacts are most commonly used. These contacts are formed by high-temperature annealing at temperatures in the range 900–1100°C, and their specific contact resistance lies typically in the range 10^{-4}–10^{-6} Ωcm^2

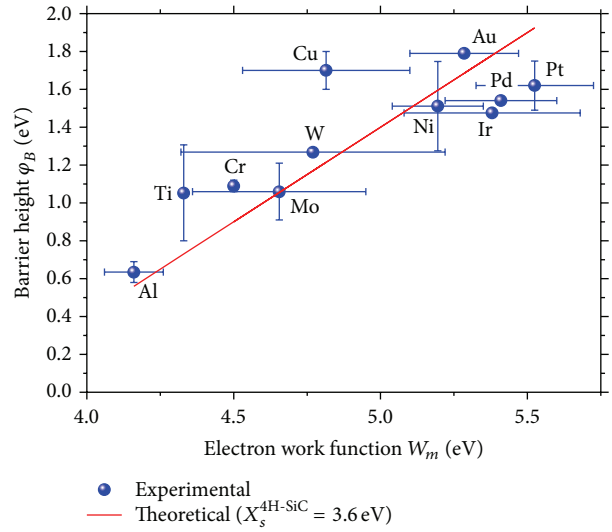

Figure 1: Experimental dependence of the barrier height φ_B of metal/4H-n-SiC on the electron work function W_m of the metals [7–23]. Red curve-theoretical dependence according to the Schottky theory (the electron affinity of 4H-SiC, X_s = 3.6 eV [25]).

[26–38]. The physical properties of Ni and the main Ni_xSi_{1-x} phases used in metallization scheme for SiC are listed in Table 1 [46–48].

Many experimental studies have been performed in order to understand the mechanism of ohmic contact formation and different models were proposed to explain the Schottky to ohmic transition; however, the final picture is still far from being complete. Indeed, in spite of a large number of publications and progress in the study of Ni and SiC interaction, there are still many open questions connected to the mechanism of contact formation and their reliability. There are different explanations in the literature concerning the mechanisms of ohmic contact formation, namely, (i) the formation of silicides [35, 39] or carbon precipitates [28, 40]; (ii) inhomogeneity of the metal/SiC Schottky barrier [41]; (iii) creation of carbon vacancies [42, 43] or defect states [44] near the interface region; and (iv) snowplow effect of dopants in the SiC substrate [45]. On the other hand, it has been commonly observed that the formation of ohmic contacts is accompanied by the interfacial reaction and/or SiC decomposition.

There is no doubt that Ni can very easily react with SiC forming a whole spectrum of nickel silicides, depending on the details of the ohmic contact fabrication process. On the other hand, there is strong evidence that the fabrication of silicides, via a contact reaction of Ni with SiC or via a deposition of the specific silicide, is not enough to produce an ohmic contact with low specific resistance. This is especially true for Ni_2Si which was firstly proposed to be responsible for the ohmic behavior but later shown to form Schottky barriers with height of 1.62–1.75 eV [41]. Also a question arises about the fate of the remaining carbon which may segregate in the contact region.

Table 1: Properties of Ni and Ni_xSi_{1-x} phases used in metallization scheme for SiC [46–48].

Phase	Resistivity ($\mu\Omega$ cm)	Melting point (°C)	Enthalpy of formation (kJ/mol)	Work function W_m (eV)
Ni	8–10	1435–1446	—	4.86 ± 0.2
Ni_2Si	20–30	1255–1318	132–143	4.46
NiSi	10–20	992	85–90	4.35
$NiSi_2$	35–50	981–993	87–94	—

As the silicide formation occurs at much lower temperatures (typically 400–600°C [49, 50]) than the transition to ohmic behavior, it has been suggested that a formation of an interfacial graphite layer is responsible for the ohmic contact formation. This hypothesis was supported by the observation of ohmic behavior of graphitized carbon on SiC [51]. On the other hand, it has been shown that [52] if even elemental C atoms may be present at the semiconductor-silicide interface at low temperatures, that is, when silicide forms, the subsequent high-temperature treatment necessary for ohmic contact formation activates carbon atoms to out-diffuse towards the top surface of the silicide. This observation has led to a hypothesis that carbon out-diffusion produces C vacancies below the contact, which act as donors for electrons and increase the net electron concentration below the contact thus reducing the barrier thickness. While the redistribution of interfacial carbon after silicide formation and its movement from the interface towards the contact surface was proven by Calcagno et al. [53], the DLTS measurements were not able to reveal the presence of a donor level related to V_C, that is, one located at 0.5 eV below the conduction-band edge [31]. Consequently, it seems that the role carbon plays in ohmic contact formation is still unclear.

Two problems related to the creation and structural evolutions of carbon in SiC-based ohmic contacts are discussed in the literature: (i) what mechanism is responsible for creation of carbon structure; (ii) location of carbon species: on the Ni-silicide/SiC interface, inside silicide layer, or on free silicide surface.

Thermal decomposition of silicon carbide results in the creation of amorphous carbon (*a*-C). The *a*-C layer appearing due to thermal 4H-SiC decomposition was already observed by means of cross-sectional transmission electron microscopy [54]. The mechanism of reaction triggered by thermal decomposition of SiC has a complex character. It includes the diffusion of carbon from the SiC interface and metal atoms (Ni) towards this interface [55]. This decomposition of silicon carbide is accompanied by the creation of Ni-silicides. The solubility of carbon and silicon atoms in silicon carbide is much lower than in Ni-silicide. Because of this, the reaction triggered by decomposition of SiC takes place in the layer deposited on silicon carbide [56]. The mobility of carbon atoms in silicide is better than the mobility of silicon atoms [56]. Because of this, the thermal decomposition of SiC covered by Ni-layer results in formation of silicide and the escape of carbon atoms from SiC/silicide interface. The complexity of the interaction between SiC and metal is also the result of the number of parameters that influence the reaction. The thickness of metal layer is one of the important factors determining the structure of carbon created during the decomposition of SiC. The investigation of interaction between 6H-SiC and Ni as a function of Ni-layer thickness showed the following [57]: (i) for a very thin Ni-layer (0.4 nm), the homogeneous carbon film appears after decomposition; (ii) for Ni-layer thickness in the range 1.6–9.6 nm, carbon flakes appear, the lateral dimensions of flakes not greater than 200 nm and their thickness in the range 5–100 graphene monolayers; (iii) for a thickness of Ni-layer above 50 nm, the carbon structure is changed to hillocks.

In view of the fact that the products of reaction between Ni and SiC at the temperature of ohmic contact formation (~1000°C) are mainly Ni_2Si and C, their role in the mechanism of ohmic contact formation needs further investigation. In this work, going further and clarifying in more detail the formation of Ni-based ohmic contact to 4H-*n*-SiC, we have investigated the influence of the layer sequence, thickness, and temperature regime on the electrical and structural properties for Ni/Si contacts to 4H-*n*-SiC. Furthermore, the fabrication of low-resistivity ohmic contacts to SiC is not sufficient for application to SiC-based devices due to their usage in harsh environments and at elevated temperatures. Here, the investigation of the reliability, for example, thermal stability of the contacts, is needed. Therefore, reliability tests were performed and are also presented in this work.

3. Experimental

3.1. Sample Preparation. *n*-type (~2×10^{17} cm^{-3}) Si-face 4H-SiC(0001) bulk wafers and *n*-type (~1×10^{19} cm^{-3}) Si-face 4H-SiC(0001) epitaxial wafers (~2.97 μm thick) from Cree Research Inc. were used. Before the deposition of the contacts, the surface was chemically cleaned by the following steps: (i) degreasing in hot organic solvents (trichloroethylene, methanol, and acetone); (ii) etching sequentially for 10 min in hot solutions of $NH_4OH : H_2O_2 : H_2O = 1:1:5$ at 65°C and $H_2O_2 : HCl : H_2O = 1:1:5$ at 70°C; and (iii) etching for 2 min in buffered HF ($HF : NH_4F : H_2O = 2:7:1$). Before each step, the samples were rinsed in deionized water and blown dry using nitrogen.

Ni, Si, and Au thin films were deposited by magnetron sputtering from Ni, Si, and Au 4N pure cylindrical targets, in an Ar plasma. Ternary Ta-Si-N diffusion barriers for contact reliability studies were prepared by reactive magnetron sputtering of a highly pure Ta_5Si_3 target in an Ar-N_2 plasma. The deposition parameters were as follows: the gas flow rate ratio during sputtering was $Ar/N_2 = 15$; the total gas pressure

was 0.6 Pa; the RF power was 250 W. The resistivity measured by the four-point probe of a 100 nm thick $Ta_{35}Si_{15}N_{50}$ film was 1 mΩ cm. The details of the heat treatment and aging are presented in Section 4.1.

3.2. Sample Characterization. The electrical characterization of the contacts involved measurements of current-voltage (*I-V*) characteristics and of the specific contact resistance (r_c). *I-V* characteristics were measured by Keithley 2400 SourceMeter using an automated setup. A circular transmission line model (c-TLM) method was used to measure r_c. The c-TLM pattern prepared by *lift-off* photolithography consists of inner contact pads with a diameter of 100 μm and a metallized area separated by rings with a space of 10, 20, 30, 45, and 60 μm. The phase composition of the contacts was investigated by X-ray diffraction (XRD) using Philips X'Pert-MPD diffractometer with a Cu K_α radiation source. The depth profile of the elements in the contacts was examined by Rutherford backscattering spectrometry (RBS) using a 1.7 MeV He^+ beam. The contact/SiC interface was observed by cross-sectional transmission electron microscope (TEM) JEM-200CX and high-resolution TEM (JEOL JEM-2100). The NanoScope IIIa atomic-force microscope (AFM) and Philips XL-30 scanning electron microscope (SEM) were used to study the surface morphology of the contact structures.

The properties of carbon species were investigated by means of micro-Raman spectrometer MonoVista 2750i. Since *D* and *G* carbon bands are rather broad, their widths are of the order of 10 cm^{-1}, and the grating with 1800 grooves/mm was used. The spectral resolution SpectraPro 2750i spectrograph with used grating was good enough to record true shapes of carbon bands. The range of Raman shift recorded during single measurement was large enough to detect both carbon bands (*D* and *G*) at the same time. As excitation green line (λ = 488 nm) from Ar^+ laser (Innova 90C FRED, Coherent Inc., USA) was used, the power of excitation was set below 1 mW on the sample in order to avoid side effects caused by absorption. The measurements were performed with irradiation of both sides of the samples. The measurements were done in the range of Raman shift from about 1200 cm^{-1} to about 1800 cm^{-1}. This range of frequencies corresponds to the main Raman bands of graphite. The spectra measured at the side of the samples covered with Ni/Si sequence of layers are treated as region of interest (ROI) spectra and they will be analyzed in this work. The spectra recorded from the side not covered with Ni/Si sequence of layers are treated as a reference. The reason for measuring the reference spectra is the occurrence of second-order Raman spectra of 4H-SiC [58] and *D* and *G* carbon bands in the same range of Raman shift. The irradiation time necessary to acquire the ROI spectra was long; in particular, it was in the range between 50 and 60 minutes. No traces of second-order Raman scattering of 4H-SiC were observed in ROI spectra. It means that second-order Raman scattering coming from 4H-SiC is below limit of detection in the case of measurements obtained from the side of the samples covered with Ni/Si sequence of layers. The reference Raman spectra are not presented in this work.

Since the intensities of *D* and *G* carbon bands were weak and the signal-to-noise ratio was not very good, the measurements in the range of Raman shift corresponding to the position of the overtone of *D* band were not performed.

In order to obtain precise information about *D* and *G*, carbon bands, ROI Raman data were analyzed by means of mathematical reconstruction of the spectra with sum of Gaussian functions. Applied procedure was described in detail in previous paper [59].

4. Results

4.1. Ni/Si Ohmic Contacts to 4H-n-SiC Bulk Wafers: Optimization of Layer Thickness, Sequence, and Temperature Regime. In order to optimize the Ni/Si-based metallizations for application as ohmic contacts to *n*-SiC, Ni/Si multilayers of different layer thicknesses and Ni-Si sequences were fabricated. The thicknesses of the Ni and Si layers were set to yield chemical compositions of the Ni-Si mixture equal to the stoichiometries of Ni-rich Ni_2Si, NiSi, and Si-rich $NiSi_2$ in the (i), (ii), and (iii) series, respectively, and as such the thicknesses were as follows: 66 nm Ni and 60 nm Si in series (i), 45 nm Ni and 100 nm Si in series (ii), and 27 nm Ni and 100 nm Si in series (iii). Furthermore, in the frames of each series, two sets of samples with different Ni-Si sequences were prepared. In the first, Si was the first deposited layer on the substrate (denoted as FL-Si) and, in the second, Ni was the first deposited layer (FL-Ni). Thus, six different sample sets were fabricated.

The films were sputter-deposited on *n*-type (~2 × 10^{17} cm^{-3}) 4H-SiC bulk wafers. The as-deposited samples were first annealed at 600°C (N_2, 15 min) when the nickel silicides phases (Ni_2Si, NiSi, and $NiSi_2$) are formed according to previous XRD results [35]. Subsequently, the samples were annealed in temperatures rising from 800 to 1100°C (N_2, 3 min) to study ohmic contact formation.

The electrical properties for all Ni/Si multilayer metallizations before and after annealing are summarized in Figure 2. Nonlinear *I-V* characteristics were observed for all as-deposited metallizations and for metallizations annealed up to 1000°C. After further annealing up to 1100°C, the *I-V* characteristics for the $NiSi_2$/*n*-SiC contacts do not change considerably, and quasi-linear *I-V* characteristics are observed for the NiSi/*n*-SiC contacts, but they remain nonohmic. The Schottky-ohmic transition was observed only for the Ni_2Si/*n*-SiC contacts after annealing at temperatures ≥1050°C. For the Ni_2Si/*n*-SiC contacts with FL-Si, a transition to a quasi-linear *I-V* characteristics and the formation of ohmic contacts with specific contact resistances $r_c \sim 4.5$ and $\sim 5.8 \times 10^{-4}$ Ω cm^2 were observed after annealing at 1050 and 1100°C, respectively. For the Ni_2Si/*n*-SiC contacts with FL-Ni, nonlinear *I-V* characteristics after annealing at 1000 and 1100°C were observed and the formation of ohmic contact with $r_c \sim 5.5 \times 10^{-4}$ Ω cm^2 was registered after annealing at 1050°C. In order to study the structure evolution during the formation of the Ni_2Si/*n*-SiC ohmic contact, as well as the influence of the type of the interfacial layer on the substrate (i.e., FL-Si or FL-Ni) on contact formation, RBS-depth profiling was performed.

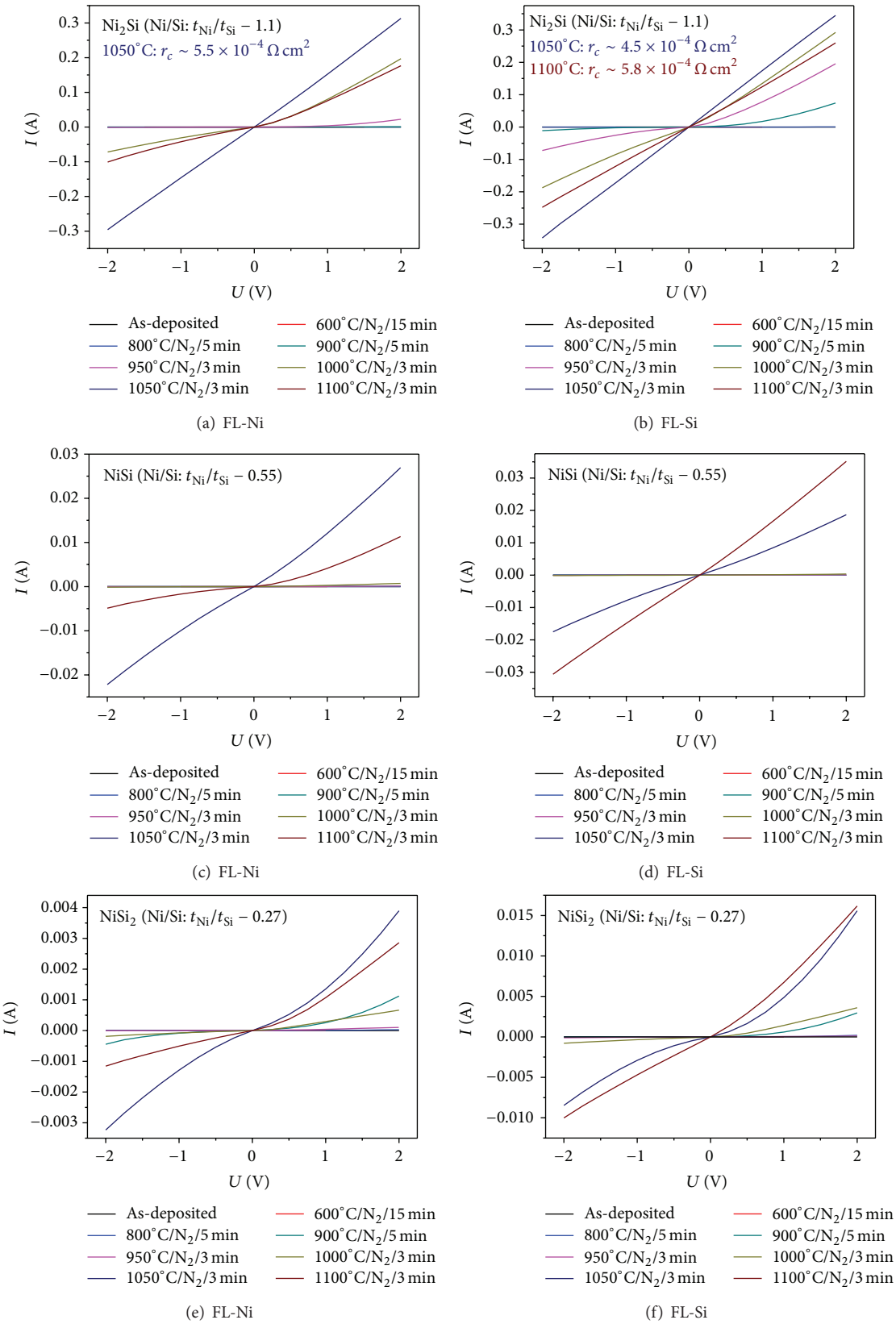

Figure 2: Electrical properties of Ni/Si multilayer contacts with different interfacial layer (Si: FL-Si or Ni: FL-Ni) and thickness ratio (t_{Ni}/t_{Si}) to n-type (~2×10^{17} cm^{-3}) 4H-SiC bulk wafers versus annealing temperature.

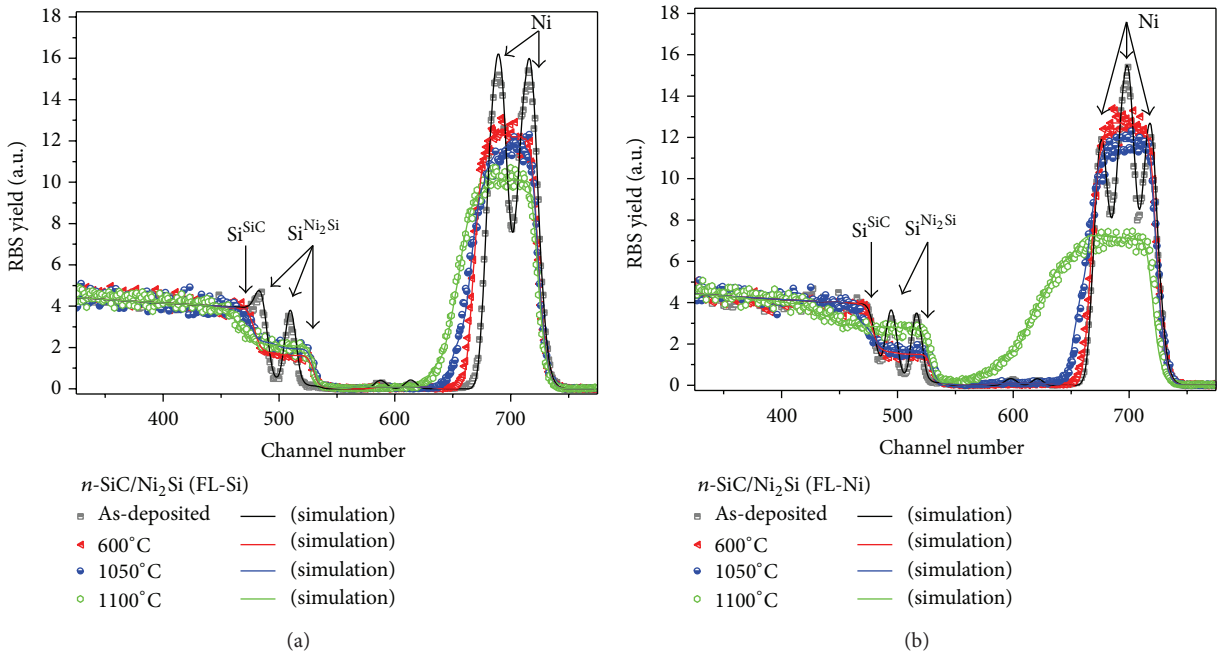

FIGURE 3: RBS spectra for as-deposited and annealed at 600°C, 1050°C, and 1100°C contacts: (a) n-SiC/Ni_2Si with FL-Si; (b) n-SiC/Ni_2Si with FL-Ni [26].

RBS profiles for the Ni_2Si/n-SiC contacts were measured after deposition and after subsequent annealing up to 1100°C. The spectra are shown in Figures 3(a) and 3(b), for samples with FL-Si or FL-Ni, respectively. The changes in the RBS profiles after annealing at 600°C for both metallization sequences indicate only a solid state reaction between the Ni and Si single layers, and no reactions at the contact/SiC interface take place. Simulations of these spectra performed using the SIMNRA code [60] confirm the formation of ~95 nm thick uniform mixtures with the atomic ratio of Ni : Si ~ 2, corresponding to stoichiometric Ni_2Si, as it was showed by XRD phase analysis [26]. Annealing of both metallization sequences at 1050°C does not induce significant changes in thicknesses or compositions of the metallizations, indicating thermal stability of the Ni_2Si phase on SiC substrates, as previously reported [33, 61, 62]. However, the very small change in the slopes of the RBS signals corresponding to Ni (Ni_2Si) and Si (SiC) measured for the metallizations annealed at 600 and 1050°C indicates a small reorganization at the metallization/SiC interface, at a maximum distance estimated at ~20 nm. SIMNRA simulations show that, for the Ni_2Si/n-SiC metallization sequences with FL-Si annealed at 1050°C, ~5 at.% of Si and C atoms out-diffused from the SiC substrate and ~10 at.% of Ni atoms diffused into SiC, whereas, for sequences with FL-Ni, ~10 at.% of Si and C out-diffused from SiC and ~20 at.% of Ni diffused into SiC. It is important to mention that this minute interaction between Ni_2Si and n-SiC after annealing at 1050°C correlates well with the Schottky-ohmic transition of contacts. Further annealing at 1100°C enhanced interdiffusion at the Ni_2Si/SiC interface. The comparison of the RBS profiles of the two metallization sequences annealed at 1100°C reveals a more pronounced reaction for the Ni_2Si/n-SiC contacts with FL-Ni (~160 nm in-depth penetration of Ni into SiC) than for the contacts with FL-Si (~40 nm in-depth penetration of Ni into SiC). This result correlates with the observed degradation of the electrical properties of the Ni_2Si/n-SiC contacts, when nonlinear I-V characteristics appear for the FL-Ni sequences, and r_c decreases for the FL-Si sequences.

The analysis of the obtained experimental results indicates that in order to form an Ni-Si-based ohmic contact to n-SiC the chemical composition of the Ni-Si layer has to be carefully controlled. Moreover, the formation of any Ni-silicides at low temperature is not sufficient to obtain ohmic contacts to n-SiC, which is in agreement with the results reported previously [8, 42, 63]. The ohmic contacts were found to be formed only by the Ni_2Si phase after high-temperature annealing (>1000°C), via a small scale interfacial reaction of Ni_2Si with SiC, which probably leads to modification of the properties of the SiC surface. The reason why the NiSi and $NiSi_2$ phases do not form ohmic contacts to n-SiC even after annealing at 1100°C is not clear. However, two approaches to explain this can be suggested based on the difference between work functions and/or melting temperatures of Ni-silicides. The compositional-induced work function tuning of Ni-silicides was previously observed and a decrease of the work function by ~0.7 eV was shown between Ni-rich and Si-rich Ni-silicides [48]. Thus, the Schottky barrier to n-SiC lowers with the transition from Ni_2Si to $NiSi_2$ contacts. Moreover, the formation of NiSi and $NiSi_2$ ohmic contacts to n-SiC with a high doping concentration (1×10^{20} cm^{-3}) after annealing at 950°C (N_2, 3 min) was previously reported [64]. Therefore, the nonohmic behavior of the NiSi and $NiSi_2$ contacts reported herein can be explained by the low doping

concentration (~10^{17} cm^{-3}) of n-SiC and the low melting temperature of about 990°C for NiSi and $NiSi_2$ bulk materials (compared to ~1318°C for Ni_2Si) [46]. The instability of the NiSi and $NiSi_2$ phases on SiC may result in Ni segregation after high-temperature annealing. In addition, the excess Si atoms from Ni-silicides probably lead to dopant deactivation via cluster formation or "neutralizing" of the donor atoms. Therefore, only a specific reaction at region near the metallization/n-SiC interface can enhance significantly the electric current through the contact. This also explains the more pronounced degradation of the electrical properties of the Ni_2Si/n-SiC ohmic contacts with FL-Ni after annealing at 1100°C.

As a result, we were able to optimize the sequence, thickness, and temperature regime for the formation of ohmic Ni/Si contacts to 4H-n-SiC. Annealing of the Ni/Si multilayers ($t_{Ni}/t_{Si} \sim 1.1$) at 600°C led to the formation of stoichiometric silicide Ni_2Si. Minimal specific contact resistances (~4.5×10^{-4} $\Omega\,cm^2$) were obtained for such Ni_2Si/n-SiC contacts with FL-Si after annealing at 1050°C. For convenience, the Ni_2Si metallizations with FL-Si are denoted as Ni_2Si below in the text.

4.2. Ni versus Ni_2Si Ohmic Contacts to 4H-n-SiC Bulk Wafers. In order to better understand the formation mechanism of Ni-based ohmic contacts to n-SiC, a comparative study of Ni versus Ni_2Si contacts on the same n-type (~2×10^{17} cm^{-3}) 4H-SiC bulk wafers annealed at similar temperatures was carried out. The properties of the as-deposited and annealed contacts are summarized in Table 2. As it was in the case of the Ni_2Si/n-SiC contacts, nonlinear I-V characteristics for Ni/n-SiC contacts were observed after annealing at temperatures between 600°C and 1000°C [38]. The Ni/n-SiC ohmic contacts are formed only after annealing at 1050°C. The specific contact resistance, r_c, was equal to ~4×10^{-4} $\Omega\,cm^2$, which is comparable to the value of 4.5×10^{-4} $\Omega\,cm^2$ obtained for Ni_2Si/n-SiC ohmic contacts annealed at 1050°C. In spite of similar electrical properties of Ni and Ni_2Si contacts, significant differences were observed in their structural properties (see Table 2). For the Ni/n-SiC contacts, the metallization thickness increases by a factor of ~2 and ~2.5 and the surface roughness increases by a factor of ~14 and ~20 after annealing at 600°C and 1050°C, respectively. For the Ni_2Si/n-SiC contacts, the metallization thickness remains unchanged and only the surface roughness increases by a factor of ~ 4 after annealing at 1050°C. In order to understand these differences between Ni and Ni_2Si contacts, XRD and RBS methods were applied to study the structural properties of the Ni/n-SiC contacts.

XRD and RBS profiles for Ni/n-SiC contacts after deposition and annealing at 1050°C are shown in Figure 4. From the XRD spectra (Figure 4(a)), we may conclude the following: (i) for the as-deposited contact, only the Ni (111) diffraction peak was detected, thus indicating the texture of the deposited film; (ii) for the contact annealed at 1050°C, only the (013) and (020) peaks of the δ-Ni_2Si orthorhombic phase were detected, thus indicating a thermally activated interaction between Ni and SiC. From the analysis of the RBS profiles (Figure 4(b)), we can deduce that annealing at 1050°C enforces diffusion of Ni atoms towards the SiC substrate and migration of Si and C atoms towards the surface. Several well-distinguished plateaus in the RBS signals for Ni and Si indicate the formation of several intermetallic compounds. SIMNRA simulations yielded the following film structure from the top surface to the substrate: firstly a 25 nm thick layer at the atomic ratio of Ni : Si ~ 2 containing ~12 at.% of C, next a 60 nm thick Ni_2Si sublayer enclosing ~26 at.% of C, subsequently a 35 nm thick mixture of ~32 at.% of Ni, ~19 at.% of Si, and ~49 at.% of C, and finally near the interface a 16 nm thick film of NiSi silicide with a smaller content of ~33 at.% of C. Significant diffusion of Ni is observed into SiC, with ~17 at.% of Ni estimated at ~40 nm in depth. The chemical composition of Ni : Si ~ 2 in the 85 nm thick top layer correlates well with δ-Ni_2Si phase identified by XRD in the sample.

The formations of nickel silicides and carbon atoms in annealed Ni/n-SiC contacts are consistent with previously reported results [33, 61]. Thus, the observed increase of metallization thickness in annealed Ni/n-SiC contacts (see Table 2) can be explained by these diffusion processes. It should be noted that the increase of metallization thickness even at 600°C indicates an interaction between Ni and SiC which is consistent with the previously reported formation of Ni-silicides at this temperature [12]. However, in spite of the reaction between Ni and SiC and the formation of Ni-silicides at just 600°C, the contacts remain rectifying up to 1050°C. Moreover, it becomes evident that the formation of the Ni_2Si phase either by an interaction between Ni and SiC, by a solid state reaction between Ni and Si single layers on n-SiC, or by a deposition of Ni_2Si layers [62] is not sufficient for the formation of an ohmic contact to n-SiC. In all of the cases, a specific interaction between the metallization and SiC is needed to change the properties of the contact/SiC near-interface region, which takes place only after annealing at high temperature (~1000°C).

This is the reason why the Ni_2Si/n-SiC and Ni/n-SiC ohmic contacts have similar $r_c \sim 4 \times 10^{-4}$ $\Omega\,cm^2$ after annealing at 1050°C. However, the quality of the Ni_2Si metallization formed as a result of the annealing of Ni/Si multilayers has a great advantage over the one formed by the annealing of the Ni single layer; namely, one can introduce a "passivating" thin Si film as the first layer (FL-Si) deposited on the SiC surface as mentioned in Section 4.1.

4.3. Microstructure and Interfacial Properties of Ni_2Si/n-SiC Contacts. In order to investigate the reaction at the metallization/SiC interface leading to the formation of ohmic contacts, XRD, AFM, and TEM techniques were applied to study the microstructure and interfacial properties of Ni_2Si/n-SiC contacts.

The results of XRD measurements performed in a Bragg-Brentano geometry, which probes through the depth of metallization, are shown in Figure 5(a). For the as-deposited Ni_2Si/n-SiC contact, only the (111) diffraction peak from textured polycrystalline Ni was detected. For the contact annealed at 600°C, the (013) and (020) peaks corresponding to the δ-Ni_2Si orthorhombic phase and the (300) peak

Table 2: Properties of Ni and Ni_2Si contacts to n-type ($\sim 2 \times 10^{17}$ cm^{-3}) 4H-SiC bulk wafers versus annealing temperature.

Annealing temperature	n-SiC/Ni			n-SiC/Ni_2Si		
	r_c ($\times 10^{-4}$ Ω cm^2)	$^*R$ (nm)	$^{**}D$ (nm)	r_c ($\times 10^{-4}$ Ω cm^2)	R (nm)	D (nm)
As-deposited	I-V: nonlinear	~3	~86	I-V: nonlinear	~3	~110
600°C/15 min	I-V: nonlinear	~40	~186	I-V: nonlinear	~4	~100
1050°C/3 min	4 ± 2	~58	~225	4.5 ± 1	~12	~108

Peak-to-valley height ($^*R$) on the 25 μm surface scan length and thickness ($^{**}D$) of metallization measured by TENCOR α-Step Profiler.

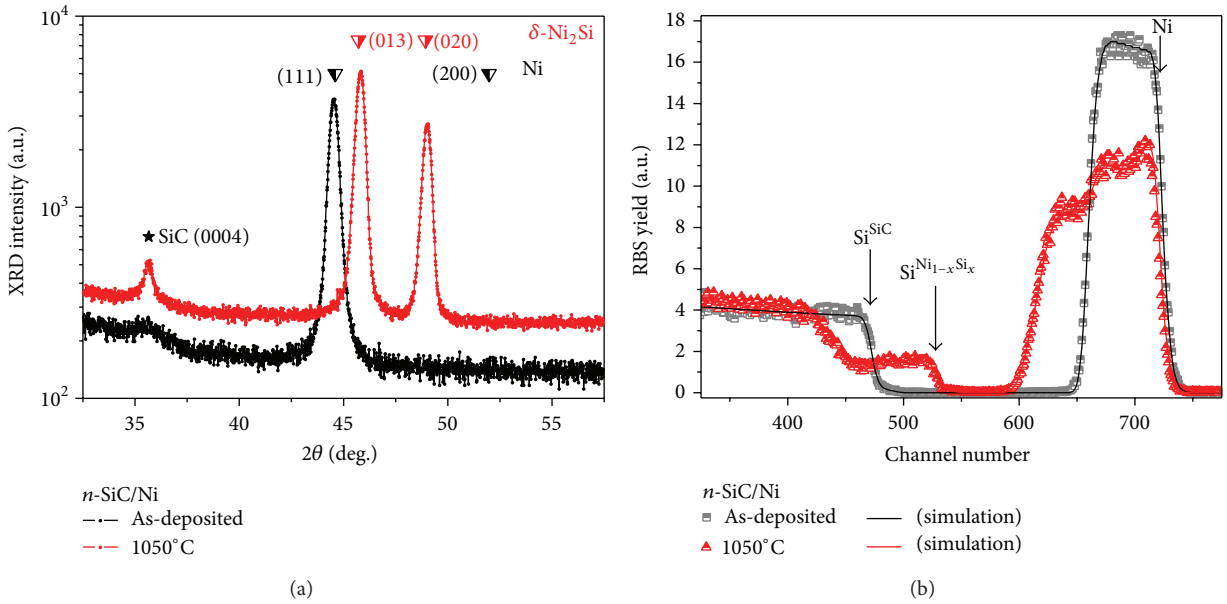

Figure 4: XRD (a) and RBS (b) spectra for as-deposited and annealed at 1050°C n-SiC/Ni (85 nm) contacts.

corresponding to the $Ni_{31}Si_{12}$ hexagonal phase are observed. Taking into account that no trace of the Ni or Si peaks appears in the XRD pattern, we conclude that a full thermally activated interaction between Ni and Si single layers took place, which is consistent with RBS results (Figure 3(a)). For the contact annealed at 950°C, only the (013) and (020) peaks of the δ-Ni_2Si phase were detected. The disappearance of the peak corresponding to the $Ni_{31}Si_{12}$ phase indicates a full transformation of other Ni-silicides into the δ-Ni_2Si orthorhombic phase. Moreover, as the intensity of the (013) peak is the highest, we can deduce a strong texturization of the δ-Ni_2Si grains. For the contact annealed at 1050°C, the (020) peak disappears leaving only the (013) peak indicating full grains texturization. However, after annealing at 1100°C, degradation of the (013) structure is visible through a significant lowering of the intensity of the (013) line and a reappearance of the (020) peak as well as the appearance of a new peak ($2\theta \approx 47.74°$) close to the (022) reflection of the Si-rich $NiSi_2$ phase. This indicates the strong interaction at the metallization/SiC interface that was also observed by RBS (Figure 3(a)). Figure 5(b) shows the intensity ratio of the (013) to (020) peaks (I_{013}/I_{020}) and FWHM (full width half maximum) for the δ-Ni_2Si (013) diffraction peak in the function of annealing temperature. A dashed horizontal line on the chart corresponds to $I_{013}/I_{020} \sim 2.5$ which is a theoretical value for a fully polycrystalline, nontextured film. The evolution of the texture can be traced from this figure as follows: after annealing at 600°C, the film is (013) textured and the preferred orientation is getting stronger with each subsequent annealing at temperatures up to 1050°C. However, after annealing at 1100°C, the ratio falls below 2.5 suggesting a random orientation of the Ni_2Si crystallites and destruction of the texture. It is clearly seen that the changes of δ-Ni_2Si (013) texture with annealing temperature correlate well with change of FWHM for δ-Ni_2Si (013), which is justified since the latter is sensitive to the perfection and size of crystallites. The texturing of the Ni_2Si phase with increasing of annealing temperature was also observed previously for Ni/n-SiC contact [65].

The surface morphology of the Ni_2Si/n-SiC contacts before and after annealing measured by AFM is shown in Figure 6. The as-deposited sample (Figure 6(a)) has a smooth surface (with peak-to-valley difference, $H \sim 6$ nm) where densely packed Ni grains of average size of 15 nm can be resolved. Annealing at 600°C causes H to increase to 13 nm and the diameter of the grains to 20 nm (Figure 6(b)). On a larger area, 30 nm high precipitates are visible originating from the interaction between Ni and Si single layers as shown earlier in RBS and XRD measurements. A strong morphology

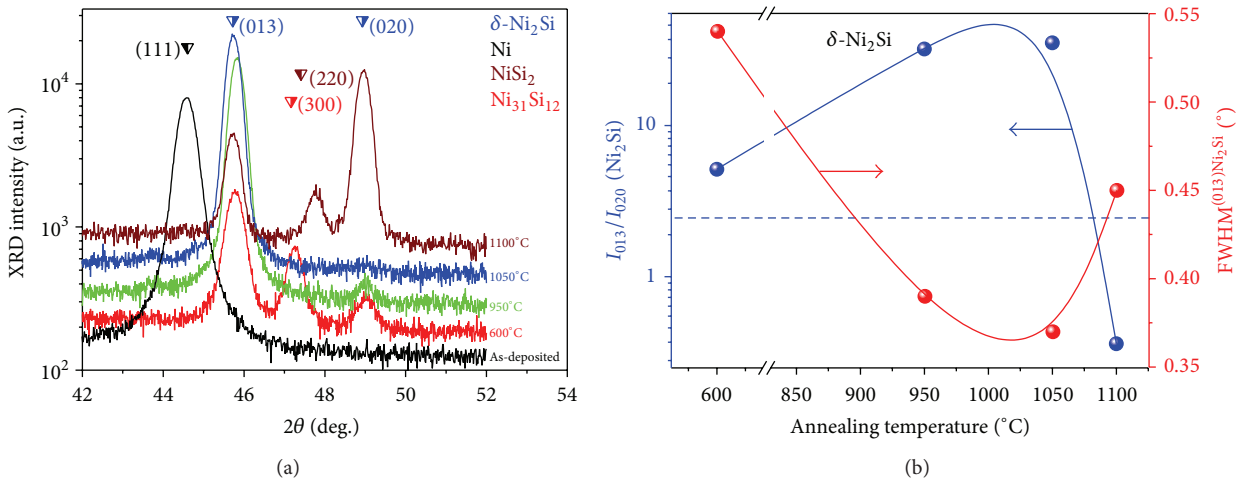

(a) (b)

FIGURE 5: (a) XRD patterns of Ni_2Si/n-SiC contacts before and after annealing at 600, 950, 1050, and 1100°C. (b) Ni_2Si texture (I_{013}/I_{020}) and FWHM of (013)Ni_2Si peak in XRD patterns versus annealing temperature (horizontal dash lines show the theoretical value for I_{013}/I_{020} in the absence of texture) [66].

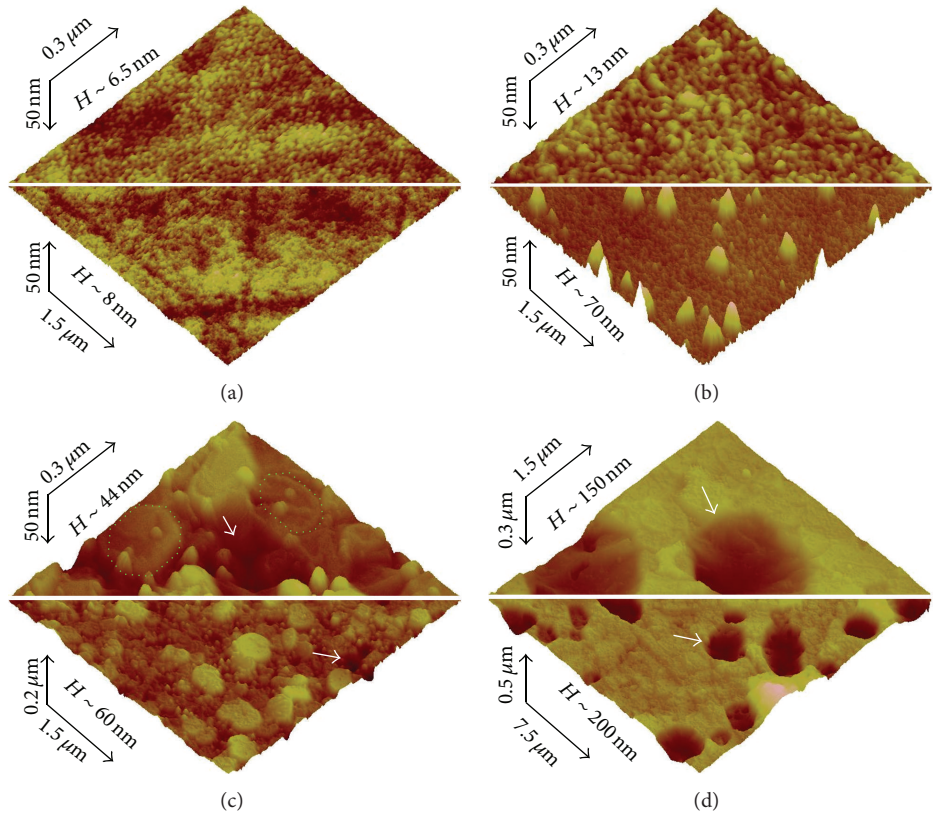

(a) (b) (c) (d)

FIGURE 6: AFM images of surface topology of Ni_2Si/n-SiC contacts before (a) and after annealing at 600°C (b), 1050°C (c), and 1100°C (d). H: surface heights ranging.

change is observed for the contact after annealing at 1050°C (Figure 6(c)). The well-defined blocks as wide as ~250 nm indicate a recrystallization of the Ni_2Si phase, which correlates well with the XRD results (Figure 5). Moreover, their spatial arrangement indicates the preferentially oriented growth. Small diameter pores of 40 nm depth can be seen between these blocks. A subsequent annealing at 1100°C degrades the morphology even more (Figure 6(d)). 140 nm deep pores appear in the film, indicating local exposition of the SiC substrate, which was also indicated in SEM measurements [67]. The pores have diameters ranging from 0.5 to 3 μm and a density ~ 0.1/μm^2.

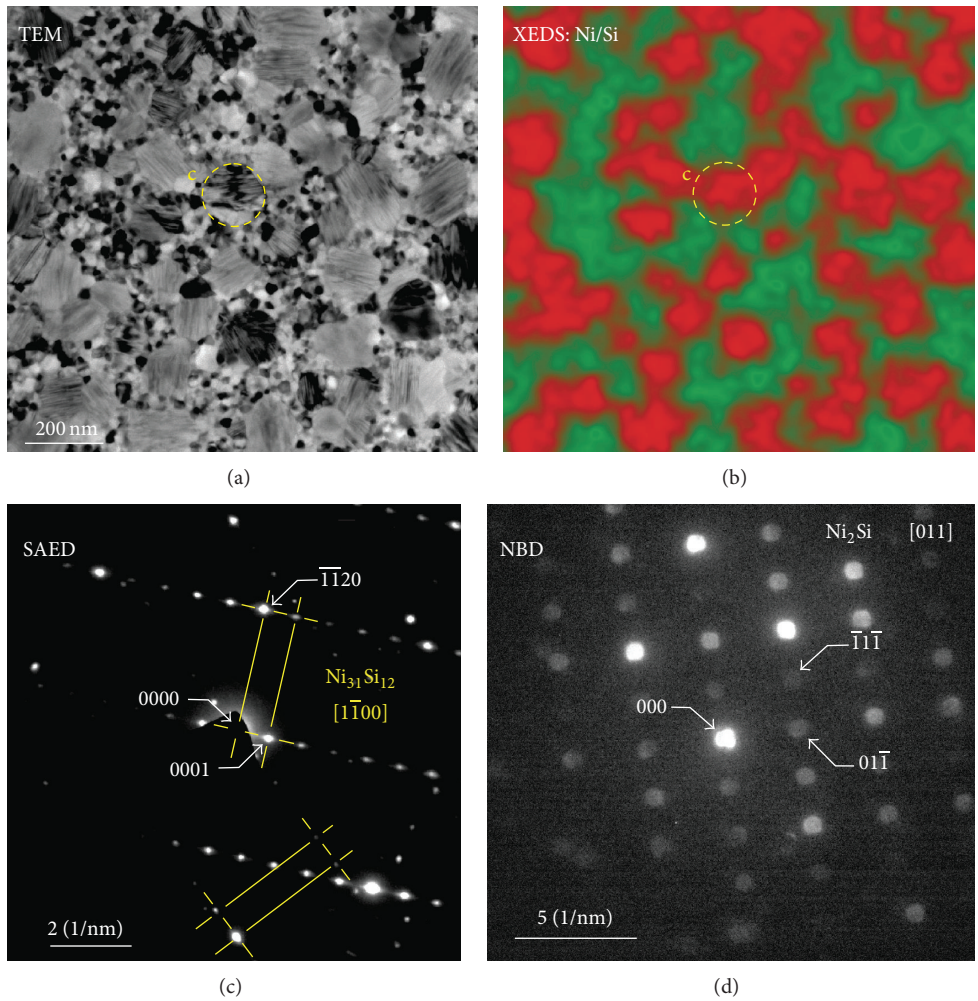

Figure 7: Results obtained from plan-view specimen of the contact annealed at 600°C: (a) plan-view TEM micrograph; (b) map representing XEDS nickel/silicon signal ratio obtained for the same area as TEM image presented in (a); (c) selected area diffraction pattern obtained for the area marked with the circle in (a) and (b); (d) NBD pattern obtained for a grain located in the area with small grains.

TEM investigations [67] of the contact annealed at 600°C showed that the metallization/SiC interface remains smooth even after a reaction between the Ni and Si single layers and the formation of a uniform polycrystalline layer (95 nm thick); this correlates well with the XRD and RBS results (Figures 3(a) and 5(a)). A plan-view TEM micrograph from the sample annealed at 600°C is presented in Figure 7(a). When considering grain sizes, the two types of grains can be distinguished. Grains of first type have sizes above 100 nm while the second-type grains are smaller with sizes up to about 50 nm. Distribution of chemical elements in the same area was investigated with X-ray energy dispersive spectrometry (XEDS). Figure 7(b) represents the map of Ni distribution divided by the map of Si after performing Gaussian averaging procedure on each map. Areas of two different chemical compositions (Ni/Si X-ray signal ratio) are clearly visible. From comparison of Figures 7(a) and 7(b), it can be concluded that "red" areas in Figure 7(b) which are the areas with higher Ni/Si XEDS signal ratio are the areas with large grains, and "green" regions, with lower Ni/Si ratio, are the regions with small grains. The circle marked in Figures 7(a) and 7(b) indicates the position of selected area diffraction (SAED) aperture, which was used to obtain diffraction pattern presented in Figure 7(c). The chosen area was in the "red" region of the XEDS Ni/Si map (Figure 7(b)), that is, in the area of higher Ni/Si XEDS signal ratio and large grains. The grains within the selected region had been oriented in the zone-axis prior to diffraction pattern acquisition. The acquired diffraction pattern indicates the crystal structure of $Ni_{31}Si_{12}$ phase (Figure 7(c)). Nanobeam diffraction (NBD) pattern obtained from a grain located in the area with small grains is presented in Figure 6(d). The pattern indicates the crystal structure of Ni_2Si phase. TEM analysis showed that in the sample annealed at 600°C $Ni_{31}Si_{12}$ and Ni_2Si grains are present. However, the presence of small grains of other phases is also possible. The sizes of the $Ni_{31}Si_{12}$ grains are significantly larger from other grains.

An exemplary cross-sectional TEM micrograph from the contact annealed at 600°C and subsequently at 1050°C is presented in Figure 8(a). The metallization consists of

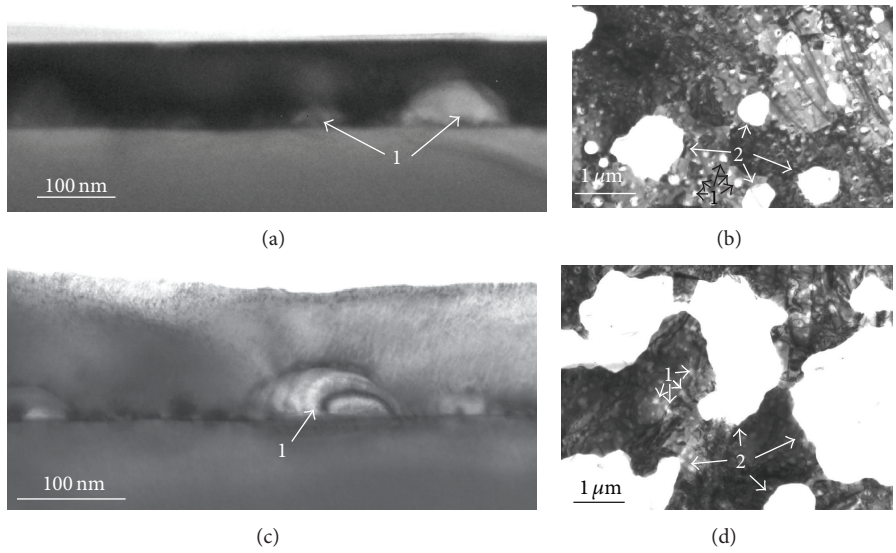

Figure 8: Cross-sectional (a, c) and plan-view (b, d) TEM micrographs obtained from Ni/Si/Ni/Si/4H-SiC contact annealed at 600°C and subsequently at 1050°C (a, b) or 1100°C (c, d). Exemplary voids are indicated with number 1 and discontinuities of the layer are indicated with number 2.

large columnar grains and voids (probably empty spaces, marked with number 1 in Figure 8) [67–69]; the height of the grains determines the contact thickness. An exemplary plan-view TEM obtained for the same contact is presented in Figure 8(b). It may be concluded that during high-temperature annealing the grains dimensions have increased; contrary to the sample annealed at 600°C, no small grains are observed. Cross-sectional and plan-view TEM micrographs from the contact annealed at 600°C and subsequently at 1100°C are presented in Figures 8(c) and 8(d), respectively. Layer discontinuities (pores) can be also distinguished in Figures 8(b) and 8(d). The possible formation mechanism of the observed voids and layer discontinuities was discussed in [69] and the method for their elimination was proposed.

In the samples annealed at 1050°C or at 1100°C, mainly the Ni_2Si phase was detected. No $Ni_{31}Si_{12}$ grains were observed. XEDS investigations revealed that, beside Ni_2Si, also some areas with higher Si content are present [70]. The metastable, high-temperature phase, denoted in the literature as θ-Ni_2Si or hexagonal Ni_3Si_2, was detected in these regions. The Ni : Si ratio in this phase can continuously change to some extent. However, it should be noted that only small part of the sample is investigated in TEM; therefore, some additions of other phases are possible.

Based on the results reported above, one may conclude that, in the investigated contacts, mainly the δ-Ni_2Si grains contribute to the electrical transport properties at the contact/SiC interface. The interface between the 4H-SiC and the δ-Ni_2Si was investigated using cross-sectional high-resolution TEM. For the contact annealed at 600°C (Figure 9(a)), an amorphous region near the interface is visible. The high-temperature annealed (1050°C) contact has a more ordered interface (Figure 9(b)) that is atomically abrupt and no contaminations or transition regions can be resolved. Moreover, in the investigated area, the absence of graphitic carbon at the interface is evident and the Ni_2Si layer is textured. The silicide lattice fringes have spacing of ~1.99 Å close to the spacing of the (013) planes of δ-Ni_2Si (~1.982 Å). They are parallel to the (0001) planes of the 4H-SiC, indicating the orientation relationship: (0001)SiC//(013) δ-Ni_2Si. This is consistent with the XRD results presented above (Figure 4(a)). Similar results were observed previously [70] for Ni/Al contacts to *n*- and *p*-type SiC after annealing at 1000°C, when a polycrystalline δ-Ni_2Si(Al) grain was found to have grown with (013) planes parallel to the (0001) plane of the SiC substrate.

4.4. Electrical Properties of Ni_2Si Contacts to 4H-n-SiC Epitaxial Wafers. As the TLM method requires that the measured contact should be placed on a thin film of the semiconductor and not on bulk in order to obtain its true electrical properties, Ni_2Si/*n*-SiC samples on *n*-type (~1×10^{19} cm^{-3}) 4H-SiC epitaxial wafers were fabricated specially for this purpose. The contacts were first annealed at 600°C (N_2, 15 min) and subsequently in temperatures rising from 900°C to 1100°C (N_2) and time rising from 3 to 12 min. For comparison, pure Ni contacts were fabricated on the same 4H-*n*-SiC epitaxial wafers and annealed at similar temperatures for 3 min.

The electrical properties of Ni and Ni_2Si contacts to 4H-*n*-SiC epi-layers before and after annealing are shown in Figure 10. The Ni/*n*-SiC ohmic contacts are formed already after annealing at 900°C (3 min). On the other hand, the Ni_2Si/*n*-SiC contacts become ohmic only after 12 min of heat treatment at this temperature. The influence of heat treatment time on the value of r_c for Ni_2Si/*n*-SiC ohmic contacts annealed at a relative low temperature (900°C) as well as at a high temperature (1100°C) is evident. This can be related with ordering changes and a reaction/interdiffusion at the contact/SiC interface after annealing at 900°C and 1100°C, respectively. The changes in r_c with annealing temperature for

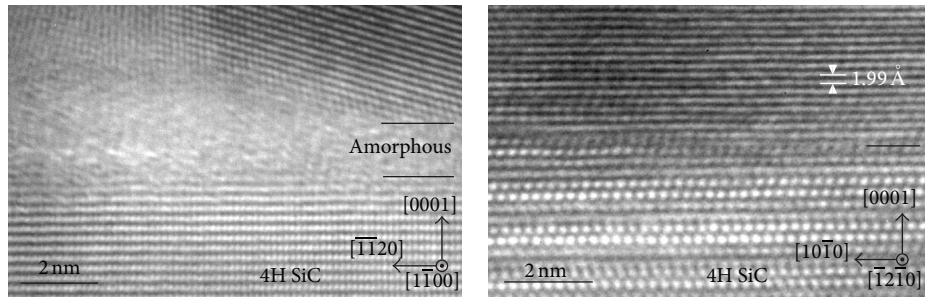

FIGURE 9: Cross-sectional high-resolution TEM images of interfacial region between the 4H-SiC substrate and the Ni-silicide after annealing at 600°C (a) and subsequently at 1050°C (b) [71].

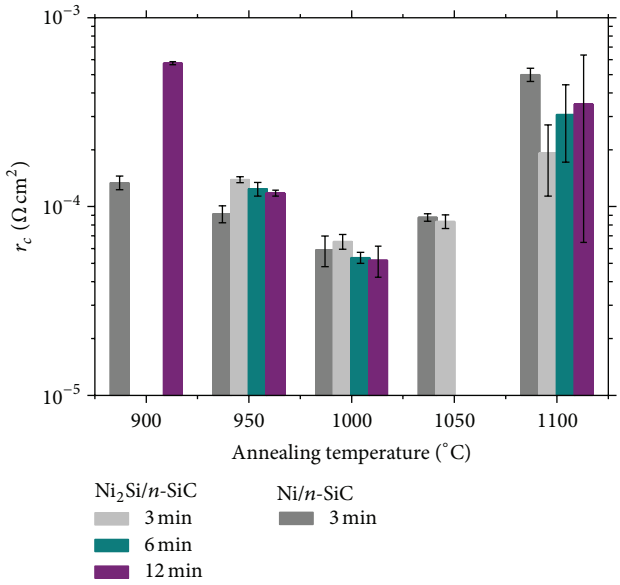

FIGURE 10: Specific contact resistances (r_c) of Ni and Ni_2Si ohmic contacts to n-type (~1×10^{19} cm^{-3}) 4H-SiC epiwafers versus annealing temperature/time.

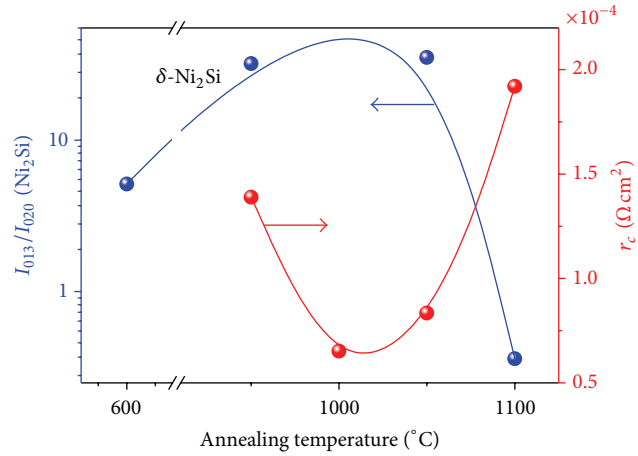

FIGURE 11: Specific contact resistances (r_c) of Ni_2Si/4H-n-SiC ohmic contacts and Ni_2Si texture (I_{013}/I_{020}) versus annealing temperature.

both contacts correlate well with the changes of texture, size, and perfection of the δ-Ni_2Si phase as shown in Figure 11. The minimal specific contact resistances $r_c \sim 5 \times 10^{-5}$ Ωcm^2 of these contacts annealed at the optimal temperature (1000°C) are lower than $r_c \sim 5 \times 10^{-4}$ Ωcm^2 of Ni and Ni_2Si ohmic contacts to low doped (~10^{17} cm^{-3}) bulk n-SiC annealed at 1050°C. It should be noted that for both the epitaxial wafer and bulk each step in the contact fabrication process was repeated identically: (i) the chemical cleaning of the surface, (ii) Ni/Si multilayers thicknesses and Ni-Si sequences. Thus, the reason why 1000°C annealing is the best for epitaxial wafer although 1050°C is the best for bulk sample can be attributed to the properties of substrates: (i) low doping concentration (10^{17} cm^{-3}) for 4H-SiC bulk wafer and high doping concentration (10^{19} cm^{-3}) for 4H-SiC epitaxial layer; (ii) better crystal quality of epitaxial layer. The difference in the doping concentration leads to the difference in the space charge region (the depletion width) for the contacts. The crystalline quality of the substrate can influence the interaction between Ni_2Si and SiC and the homogeneity of contact interface at nanoscale. Based on this, we can explain the difference in optimal annealing temperature between bulk and epitaxial wafers for lowest contact resistance and barrier height. Moreover, we think this is also the reason that for 4H-SiC epitaxial layer contact becomes ohmic after annealing at 950°C but for 4H-SiC bulk wafer only after annealing at 1050°C.

In order to determine the relative importance of the electron transportation mechanisms at the interface between the contact and semiconductor, it is necessary to calculate the magnitude of the Padovani-Stratton parameter E_{00} given by [72]

$$E_{00} = \frac{qh}{4\pi}\sqrt{\frac{N_d}{m^*\varepsilon}}, \quad (1)$$

where h is Planck's constant, m^* is the effective mass of the electron in the semiconductor, ε is semiconductor dielectric constant, and N_d is the donor concentration. The size of E_{00} with respect to kT gives an indication of the relative importance of field emission (FE, $E_{00}/kT \gg 1$), thermionic field emission (TFE, $E_{00}/kT \sim 1$), or thermionic emission

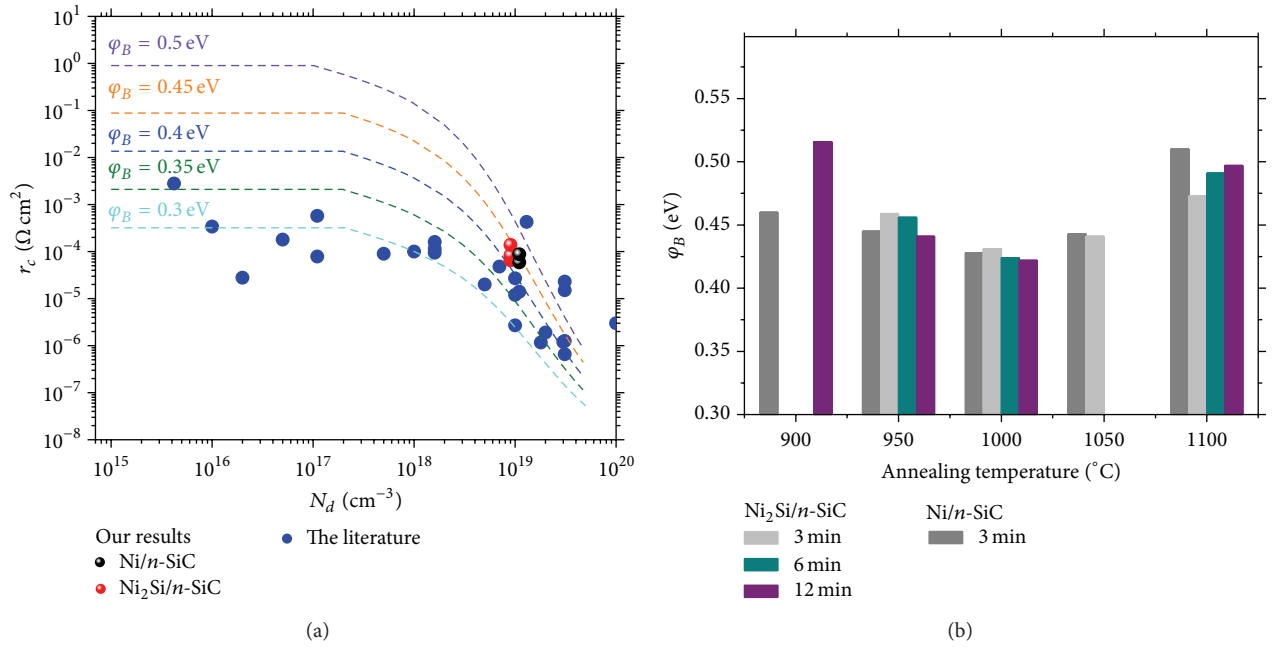

(a) (b)

FIGURE 12: (a) Calculated ohmic contact resistance (r_c) as a function of the doping concentration (N_d) of 4H-n-SiC for various barrier heights (φ_B). The lines represent the calculated dependences based on the TE and TFE models. The points represent the experimental data for contacts annealed at 950, 1000, and 1050°C for 3 min as well as some data from [7–47]. (b) Effective barrier height (φ_B) of Ni and Ni$_2$Si ohmic contacts to n-type (~1 × 10^{19} cm^{-3}) 4H-SiC epiwafers versus annealing temperature/time.

(TE, $E_{00}/kT \ll 1$) [73]. In our case (n-type 4H-SiC) and at our maximum doping level of 1×10^{19} cm^{-3}, $m^* = 0.36m_0$, and $\varepsilon = 9.66\varepsilon_0$, E_{00} was found to be about 31.5 meV. A comparison of E_{00} to the thermal energy kT shows thermionic field emission to dominate ($E_{00}/kT = 1.25$). The FE model is the dominant mechanism for the ohmic contact to a degenerated semiconductor.

The barrier heights of the contacts after annealing were estimated by comparing the theoretical and measured contact resistances. Since the density of states in the conduction band of 4H-SiC is >1×10^{19} cm^{-3} [74], samples used here were not degenerated because of $n \sim 1 \times 10^{19}$ cm^{-3}. Therefore, we calculated the theoretical curve for the carrier concentration dependence of the specific contact resistance by using the TE and TFE models.

According to the TE, the specific contact resistance is calculated by [72]

$$r_c = \frac{kT}{qA^*} \exp\left(\frac{\varphi_B}{kT}\right), \quad (2)$$

where φ_B is barrier height and A^* (= 146 A cm^{-2} K^{-2} for 4H-SiC [75]) is the Richardson constant.

According to the TFE, the specific contact resistance is calculated by [73]

$$r_c = \frac{k^2}{qA^* \sqrt{\pi(\varphi_B + u_F) E_{00}}} \cosh\left(\frac{E_{00}}{kT}\right) \sqrt{\coth\left(\frac{E_{00}}{kT}\right)} \cdot \exp\left(\frac{\varphi_B + u_F}{E_0} - \frac{u_F}{kT}\right), \quad (3)$$

where $E_0 = E_{00} \coth(E_{00}/kT)$ and $\mu = kT \ln(N_c/N_d)$, where N_d is the donor concentration and N_c is effective density of states in conduction band.

In Figure 12(a), the theoretical specific contact resistances r_c of ohmic contacts to 4H-n-SiC are plotted as a function of the doping concentration (N_d) and barrier height (φ_B) ranging from 0.3 eV to 0.5 eV. The quantitative agreement of theoretical, our experimental, and previously reported values of r_c is evident. The measured variation of r_c for Ni and Ni$_2$Si ohmic contacts with annealing temperature/time shows different values of the effective barrier height (φ_B) as shown in Figure 12(b). The minimal values of $\varphi_B \sim 0.42 \pm 0.3$ eV for Ni$_2$Si(Ni)/n-SiC ohmic contacts annealed at 1000°C correlate well with values of $\varphi_B \sim 0.42$ eV previously reported for Ni contacts to n-type 4H-SiC annealed at 1100°C [76].

Thus, the changes of r_c and microstructure of δ-Ni$_2$Si phase with annealing temperature for Ni$_2$Si/n-SiC ohmic contacts were correlated with the changes of effective barrier height (φ_B) at the contact/SiC interface. This explains the similar electric properties of the Ni$_2$Si/n-SiC and Ni/n-SiC contacts and high-temperature annealing (~1000°C) needed for ohmic contact formation.

4.5. The Role of SiC Decomposition in the Formation of Ni-Based Ohmic Contacts. Figure 13 presents the data obtained for the Ni$_2$Si/n-SiC contacts with FL-Si annealed at different temperatures. The signal presented in Figure 13(a) can be modeled using a sum of three Gaussian functions. The main component has the maximum at 1587 cm^{-1} and FWHM equal to 579 cm^{-1}. Two other Gaussian profiles have the maxima at

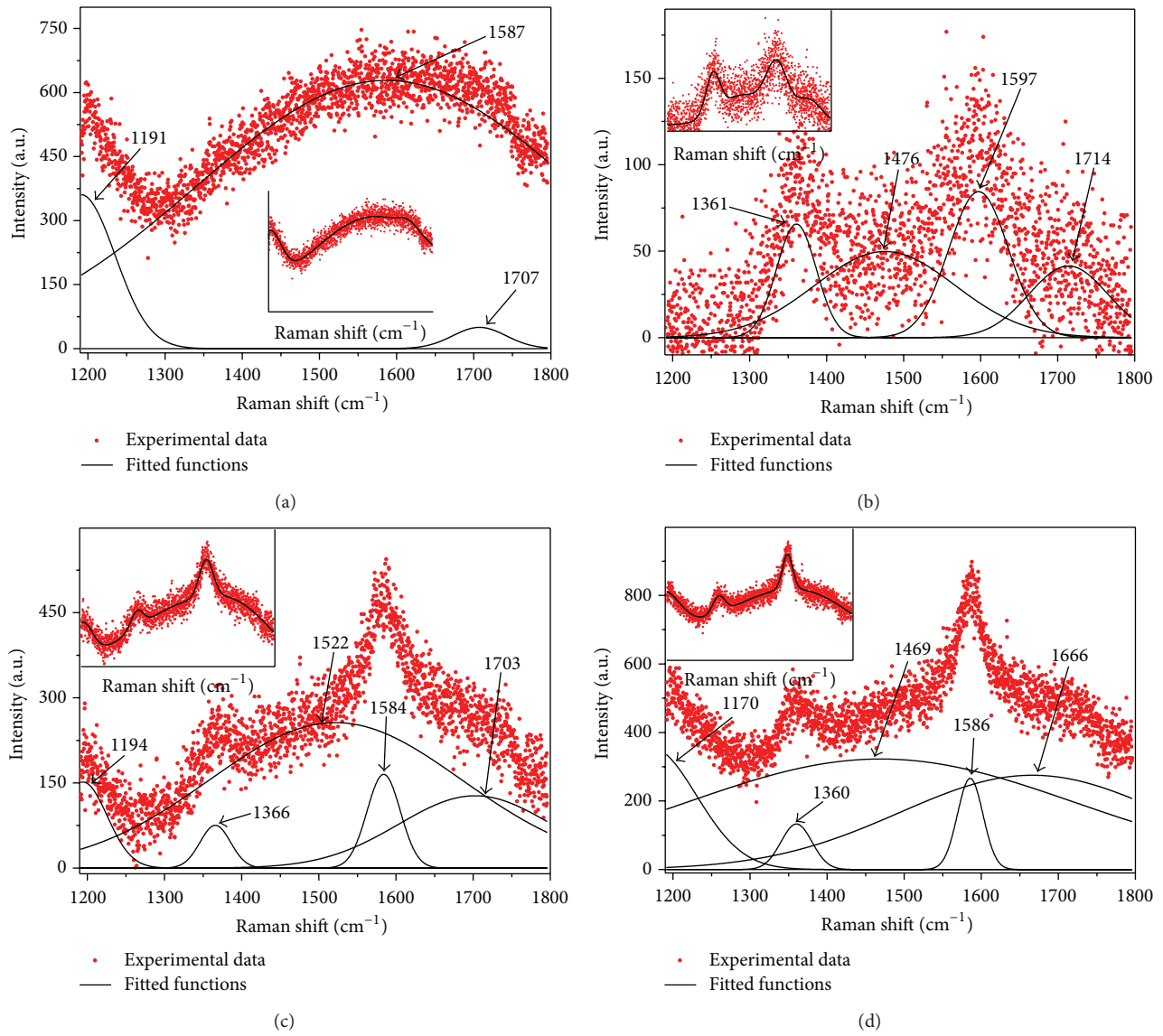

FIGURE 13: Raman spectra recorded for the Ni_2Si/n-SiC contacts with FL-Si after different thermal treatment: (a) as-deposited; (b) 600°C/15 min; (c) 950°C/3 min; (d) 1050°C/3 min.

1191 cm^{-1} and 1707 cm^{-1} and FWHM equal to 105 cm^{-1} and 81 cm^{-1}, respectively.

In the case of the experimental data shown in Figure 13(b), four Gaussian functions are necessary to get proper shape of the spectrum. The maxima of the Gaussian functions have the following positions: 1361 cm^{-1}, 1476 cm^{-1}, 1597 cm^{-1}, and 1714 cm^{-1}. The corresponding values of FWHM are equal to 61 cm^{-1}, 215 cm^{-1}, 91 cm^{-1}, and 121 cm^{-1}.

The data presented in Figures 13(c) and 13(d) require five Gaussian profiles to obtain proper mathematical reconstruction of the spectrum. Three profiles can be recognized as relatively narrow and two others, as broad. The first *narrow* Gaussian component has the maximum placed at 1194 cm^{-1} in the case of the spectrum presented in Figure 13(c) and 1170 cm^{-1} for the spectrum shown in Figure 13(d). The corresponding FWHM values are equal to 74 cm^{-1} and 142 cm^{-1}, respectively. The next *narrow* profiles are placed around 1366 cm^{-1} in the case of spectrum from Figure 13(c) and 1360 cm^{-1} for spectrum from Figure 13(d). The values of FWHM are almost equal for both Gaussian profiles. The exact values are 47 cm^{-1} and 48 cm^{-1} for spectra from Figures 13(c) and 13(d), respectively. The third *narrow* profile has the maximum at 1584 cm^{-1} in the case of spectrum from Figure 13(c) and at 1586 cm^{-1} for Figure 13(d). The value of FWHM is in the case of Gaussian function from Figure 13(d) much smaller in comparison with the same function from Figure 13(c). The FWHM of Gaussian profile from Figure 13(c) is equal to 51 cm^{-1}. The same parameter obtained for the spectrum presented in Figure 13(d) is equal to 39 cm^{-1}. *Broad* Gaussian profiles can be divided into two pairs. The components of the first pair have the maxima placed between bands reproduced

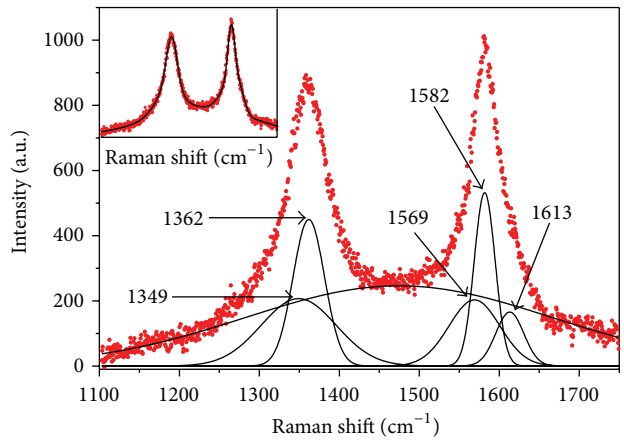

FIGURE 14: Raman spectrum recorded for Ni/*n*-SiC contact annealed at 1050°C.

by second and third *narrow* Gaussian functions. The values obtained from fitting procedure are equal to 1522 cm^{-1} and 1469 cm^{-1} for spectra from Figures 13(c) and 13(d), respectively. Both Gaussian functions have large FWHM. They are equal to 385 cm^{-1} and 594 cm^{-1} for profiles from Figures 13(c) and 13(d), respectively. The last pair is composed of Gaussian functions centered at 1703 cm^{-1} in the case of Figure 13(c) and at 1666 cm^{-1} for Figure 13(d). The corresponding FWHM values are equal to 234 cm^{-1} and 404 cm^{-1}.

Figure 14 presents the reference spectrum measured for a Ni-layer deposited on *n*-SiC substrate (Ni/*n*-SiC contact) and annealed at 1050°C. The signal-to-noise ratio is in the case of this spectrum much better in comparison with any spectrum from Figure 13. Six Gaussian functions are necessary for proper reconstruction of the spectrum. The first profile has the maximum at 1474 cm^{-1} and FWHM equal to 450 cm^{-1}. The maximum of this profile is not given in the plot. The last Gaussian function has the maximum at 1613 cm^{-1} and FWHM equal to 41 cm^{-1}. Four remaining Gaussian profiles can be divided into two pairs of *narrow* and *broad* functions. The pair of *broad* profiles has the maxima at 1349 cm^{-1} and 1569 cm^{-1}. The corresponding FWHM values are equal to 110 cm^{-1} and 75 cm^{-1}. The *narrow* Gaussian functions are centered at 1362 cm^{-1} and 1582 cm^{-1}. The values of FWHM are equal to 47 cm^{-1} and 31 cm^{-1}, respectively. Parameters obtained from mathematical reconstruction of Ni/*n*-SiC contact annealed at 1050°C are summarized in Table 3.

The focus of this paragraph is on carbon structures created due to thermal processes. The first bands which can be assigned to the vibrations related to carbon structures have to be selected. The following bands can be treated as background not directly related to carbon: (i) Figure 13(a), bands centered at 1191 cm^{-1}, 1587 cm^{-1}, and 1707 cm^{-1}; (ii) Figure 13(b), bands centered at 1476 cm^{-1} and 1714 cm^{-1}; (iii) Figure 13(c), bands centered at 1194 cm^{-1}, 1522 cm^{-1}, and 1703 cm^{-1}; (iv) Figure 13(d), bands centered at 1170 cm^{-1}, 1469 cm^{-1}, and 1666 cm^{-1}; (v) Figure 14, band centered at 1474 cm^{-1}.

In the case of Figures 13(a), 13(c), and 13(d), the first Gaussian profile (maximum placed below 1200 cm^{-1}) is relatively narrow. However, the maximum of this function is placed outside the measured range of Raman shift. Since only a part of the fitted Gaussian profile lies on experimental points in the measured spectrum, the position of the function can be inaccurate. The bands, (i) 1587 cm^{-1} from Figure 13(a); (ii) 1476 cm^{-1} from Figure 13(b); (iii) 1522 cm^{-1} and 1703 cm^{-1} from Figure 13(c); (iv) 1469 cm^{-1} and 1666 cm^{-1} from Figure 13(d); (v) 1474 cm^{-1} from Figure 14, have large FWHM values which exceeded 200 cm^{-1}. The band centered at 1707 cm^{-1} in Figure 13(a) has small contribution to the spectrum. The band at 1714 cm^{-1} in Figure 13(b) contributes significantly. However, the signal-to-noise ratio is in this case unfavorable, so only the most distinct features of the spectrum can be treated as reliable. The above arguments suggest that all the above-mentioned Gaussian profiles contribute rather to the background although some of them can be correlated with carbon structures; in particular, (i) bands 1476 cm^{-1} in Figure 13(b) and 1469 cm^{-1} from Figure 13(d) can be correlated with vibrations of polyene [77]; (ii) band 1522 cm^{-1} in Figure 13(c) can be correlated with amorphous carbon [77]. The other bands can be assigned to the products related to silicon carbide decomposition.

In the case of the reference sample five bands are related to the thermal decomposition of silicon carbide. The band characterized by the maximum placed at 1613 cm^{-1} with FWHM equal to 41 cm^{-1} can be assigned to Nickel-Graphite Intercalation Compounds (Ni-GIC) [77]. The formation of metal intercalation compounds during catalytic graphitization of 4H-SiC in the presence of nickel, cobalt, chromium, or other metals and at the temperature 800°C or higher was already described in detail [77].

The other bands indicated in Figures 13 and 14 can be assigned to *D* and *G* vibrations reported for carbon structures [78]. The most important features, (i) maxima positions; (ii) full width at half maximum (FWHM); and (iii) *D*-to-*G* intensity ratio ($I(D)/I(G)$) of the bands obtained for the Ni_2Si/*n*-SiC contacts annealed at 600, 950, and 1050°C, are summarized in Table 4. The bands obtained for the Ni_2Si/*n*-SiC contact after annealing at 600°C suggest a microcrystalline character of the carbon. This is reflected in the position of the *G* band, which is shifted higher than the standard position reported for graphite [79]. The band centered at 1597 cm^{-1} and FWHM equal to 91 cm^{-1} is typical for Raman spectra of microcrystalline carbon. The one observed in this case is a combination of pure *G* band and the band centered at about 1620 cm^{-1} and assigned to double C=C bonds and marked in the literature as D' [77]. The bands are merged in such a way that it is impossible to separate them. Large values of FWHM obtained for both carbon bands equal to 61 cm^{-1} and 91 cm^{-1} for *D* and *G* bands suggest large scattering of the structural parameters of carbon species.

In the case of the Ni_2Si/*n*-SiC contact annealed at 950°C maximum of *D* band is shifted towards larger values of Raman shift by 5 cm^{-1} Ni_2Si/*n*-SiC contact after annealing at 600°C. The shift points to the increase of the thickness of the carbon layer with increasing annealing temperature from

Table 3: Properties of D and G bands recorded for reference Ni/n-SiC contact.

Sample	D band		G band		$I(D)/I(G)$
	Maximum [cm^{-1}]	FWHM [cm^{-1}]	Maximum [cm^{-1}]	FWHM [cm^{-1}]	
Ni, broad	1349	110	1569	75	1.02
Ni, narrow	1362	47	1582	31	0.85

Table 4: Properties of D and G bands observed for the Ni_2Si/n-SiC contacts annealed at 600, 950, and 1050°C.

Sample	D band		G band		$I(D)/I(G)$
	Maximum [cm^{-1}]	FWHM [cm^{-1}]	Maximum [cm^{-1}]	FWHM [cm^{-1}]	
600°C	1361	61	1597	91	0.78
950°C	1366	47	1584	51	0.46
1050°C	1360	48	1586	39	0.50

600 to 950°C. Such an effect was already observed for the overtone of D band – 2D [80]. The FWHM of D and G bands in the case of the Ni_2Si/n-SiC contact annealed at 950°C are smaller than after annealing at 600°C. The reduction of FWHM values for both carbon bands suggests a more homogeneous structure of carbon species in the Ni_2Si/n-SiC contact annealed at 950°C. This is consistent with the decrease of $I(D)/I(G)$ intensity ratio obtained for samples Ni_2Si/n-SiC contact after annealing at 600°C and the Ni_2Si/n-SiC contact annealed at 950°C. The values of D-to-G intensity ratio equal to 0.78 and 0.45 for the Ni_2Si/n-SiC contact annealed at 600 and 950°C, respectively, point to a higher graphitization degree in the case of second sample. The maximum of G band is equal to 1584 cm^{-1}, the standard value reported for graphite [78].

D and G bands obtained for the sample with the Ni_2Si/n-SiC contact annealed at 1050°C have the maxima positions equal to 1360 cm^{-1} and 1586 cm^{-1}, respectively. The bands are shifted in opposite directions in comparison with bands observed for sample Ni_2Si/n-SiC contact annealed at 950°C; in particular, D band is shifted towards smaller values of Raman shift by 6 cm^{-1} and G band towards larger frequencies by 2 cm^{-1}. This type of change was already reported for increase of the content of ABA stacking order in comparison with ABC stacking order [81]. ABC stacking order is preferentially formed during thermal decomposition of silicon carbide especially at temperatures below 1000°C [82]. The FWHM of D band is in the case of the Ni_2Si/n-SiC contact annealed at 1050°C almost the same as for the Ni_2Si/n-SiC contact annealed at 950°C (48 cm^{-1} versus 47 cm^{-1}). These values point to similar distribution of structural parameters for defected structures in both samples. Significant reduction of FWHM for G band, in particular from 51 cm^{-1} for the Ni_2Si/n-SiC contact annealed at 950°C to 39 cm^{-1} for the Ni_2Si/n-SiC contact annealed at 1050°C, suggests more homogeneous structure of carbon species in the Ni_2Si/n-SiC contact annealed at 1050°C.

The parameters of the D and G bands obtained from mathematical analysis of reference sample (Ni/n-SiC) are collected in Table 3. The bands are divided into two groups. The first one is composed of the D and G narrow bands; the other group consists of D and G broad bands. The pair of narrow bands observed for the reference sample is similar to the D and G bands obtained for the Ni_2Si/n-SiC contact annealed at 1050°C sample. Small shift of the maxima positions, in particular (i) by 2 cm^{-1} towards larger values of Raman shift for D band (1362 cm^{-1} versus 1360 cm^{-1}) and (ii) by 4 cm^{-1} towards smaller values of Raman shift in the case of G band (1582 cm^{-1} versus 1586 cm^{-1}), can be correlated with different stacking order for both samples. The shift of both bands as described above suggests a larger contribution of ABC stacking order in reference sample than in the Ni_2Si/n-SiC contact annealed at 1050°C [81]. The value of FWHM for D narrow band is almost the same as in the case of D band observed for the Ni_2Si/n-SiC contact annealed at 1050°C. It points to almost the same distribution of structural parameters for both samples. Significantly smaller FWHM value of G band for reference sample (31 cm^{-1} versus 39 cm^{-1}) suggests a more homogeneous structure of graphite species in Ni/n-SiC sample than in the Ni_2Si/n-SiC contact annealed at 1050°C. D-to-G intensity ratio is equal to 0.85 in the case of narrow bands in reference sample. This value is larger than $I(D)/I(G)$ obtained for any sample from series: Ni_2Si/n-SiC contact after annealing at 600°C, the Ni_2Si/n-SiC contact annealed at 950°C, and the Ni_2Si/n-SiC contact annealed at 1050°C. The value of D-to-G intensity ratio points to smaller graphitization degree of Ni/n-SiC sample than even in Ni/Si/Ni/Si/n-SiC sample annealed at 600°C during 15 min.

The other D and G bands form the pair of broad bands. Both broad bands are shifted towards lower frequencies by 13 cm^{-1} in comparison with narrow bands. The position of D and G band as observed for the broad pair suggests the nanocrystalline graphite mixed with sp^3 phase. The content of sp^3 phase should be about 10% [77, 78]. FWHM obtained for D band points to large distribution of structural parameters in defected structures. It is almost twice as large as the value obtained for the Ni_2Si/n-SiC contact after annealing at 600°C. The value of FWHM obtained for the G broad band is placed between the values for Ni_2Si/n-SiC contact after annealing at 600°C and the Ni_2Si/n-SiC contact annealed at 950°C. It means that the homogeneity of graphite structure is better than for Ni_2Si/n-SiC contact after annealing at 600°C sample but worse than for the Ni_2Si/n-SiC contact annealed at 950°C.

Graphitization degree defined as $I(D)/I(G)$ is a commonly used qualitative description of the carbon species. The evolution of graphite structure can be divided into three stages [79]: (i) graphite (*g*-C) → nanocrystalline graphite (*nc*-C); (ii) *nc*-C → amorphous carbon (*a*-C); (iii) *a*-C → tetrahedral *a*-C (*ta*-C). In the 1st stage, the reduction of phonon correlation length can be described by the following formula: $I(D)/I(G) \sim {L_a}^{-1}$, where L_a is called "in-plane correlation length" and can be identified with the dimension of graphite grain [78, 79]. The proportionality constant is dispersive; for example, for wavelength equal to 514.5 nm (green line of Ar^+ laser), this constant is equal to 44 Å [78]. The same value of proportionality constant can be used for another important Ar^+ laser line: 488 nm [83]. The formula is valid down to $L_a \approx (2 \div 3)$ nm [83]. Since the graphite is not uniformly nanocrystalline, the grain dimension obtained from Raman spectra should be taken as a mean value. The maximum position of *G* band moves in this stage from about 1580 cm^{-1} to about 1600 cm^{-1}.

In the 2nd stage, the *D* and *G* bands evolve gradually to the broad single band typical for *a*-C [79]. The dimension of the grains is smaller than 2 nm. The *D*-to-*G* intensity ratio is in this stage proportional to ${L_a}^2$ and the proportionality constant for green line of Ar^+ laser (514.5 nm) is equal to 0.0055 [83]. In the 3rd stage, $I(D)/I(G) \approx 0$ [79].

Taking into account $I(D)/I(G)$ from Tables 3 and 4, one can calculate the following grain sizes for all species contributing to Raman spectra: (i) Ni_2Si/*n*-SiC contact after annealing at 600°C (5.6 nm), at 950°C (9.6 nm), and at 1050°C (8.8 nm); (ii) Ni/*n*-SiC contact after annealing at 1050°C (narrow bands, 5.2 nm, and broad bands, 4.3 nm). Above-calculated grain dimensions show that carbon species observed in samples investigated in this work can be divided into three groups: (i) Ni_2Si/*n*-SiC contact after annealing at 950°C and Ni_2Si/*n*-SiC contact after annealing at 1050°C; (ii) Ni_2Si/*n*-SiC contact after annealing at 600°C and Ni/*n*-SiC contact after annealing at 1050°C (narrow bands); (iii) Ni/*n*-SiC contact after annealing at 1050°C (broad bands). Furthermore, it can be seen that Ni metallization results in creation of carbon grain with smaller size than Ni/Si metallization although the amount of carbon appearing due to silicon carbide decomposition is significantly larger.

Thus, the deposition of Ni/Si/Ni/Si sequence of layers combined with annealing at 600°C results in creation of a silicide layer with negligible decomposition of SiC [26, 38]. The intensities of *D* and *G* bands increase with the increase of the annealing temperature. This is clearly visible in Figure 13. Annealing at higher temperature after creation of silicide layer slows down the process of thermal decomposition. The intensities of *D* and *G* bands in the case of Ni_2Si/*n*-SiC contacts are significantly smaller than the intensities of these bands obtained for the reference sample (Ni/*n*-SiC). In the case of Ni_2Si/*n*-SiC contact, the initial structure built from sequence of silicon and nickel layers results in the fast formation of a silicide. In the case of the Ni/*n*-SiC contact catalyzed by Ni decomposition, the decomposition of larger amount of SiC is observed. This is confirmed by results from Raman measurements and other techniques. Raman spectra recorded for the reference sample point to larger amount of carbon in comparison with samples Ni_2Si/*n*-SiC. On the other hand, the quality of the carbon formed in the sample Ni_2Si/*n*-SiC (1050°C) is much higher than in reference sample as proven by the graphitization degree reflected in $I(D)/I(G)$ ratio and by scattering of structural parameters visible in FWHM of the bands.

The other problem is the location of carbon species. In the case of Ni_2Si/*n*-SiC contacts, the rate of decomposition is small. Experimental techniques like XRD or HRTEM did not detect traces of carbon either on the SiC/silicide interface or in the silicide layer. Moreover, the intensities of Raman spectra recorded for these contacts are very low and the concentration of carbon species may be not detectable by XRD. The situation looks different for the Ni/*n*-SiC contact. A mathematical analysis of the Raman spectra points to two different types of carbon. Each type is characterized by the pair of *D* and *G* bands. The pair of broad bands should characterize the carbon species appearing on SiC/silicide interface. Large values of FWHM suggest large scattering of structural parameters. This situation is typical for carbon formed during thermal decomposition of silicon carbide. The other pair of bands, called narrow, corresponds to the second type of carbon. The FWHM values suggest scattering of structural parameters comparable with the Ni_2Si/*n*-SiC (1050°C) sample. *D*-to-*G* ratio points to lower graphitization degree in comparison with Ni_2Si/*n*-SiC (1050°C) sample although the annealing of both samples was done at the same temperature.

Lower graphitization degree together with higher decomposition ratio in the case of reference sample results from different metallization. In the case of the Ni/Si sequence of layers, Ni is mixed with Si and silicides can be created almost without decomposition of SiC substrate. Metallization with single Ni layers requires SiC decomposition in order to get the Si necessary to form the silicide layer. Decomposition of a large volume of the SiC substrate results on the other hand in a larger carbon presence. This carbon diffuses from the interface to the silicide surface where the graphite layer with relatively high graphitization degree is created. This is in agreement with the data reported in the literature [84] which suggest that the thermal treatment above 1000°C accelerates decomposition of silicon carbide and diffusion of carbon from interface area. Creation of graphite layer on the free silicide surface in the case of reference sample is supported by data presented in this work and obtained from other experimental techniques. For example, investigation with high-resolution TEM did not detect the traces of carbon structures at the interface between silicide layer and SiC substrate.

The other problem is the location of carbon species responsible for the "broad" pairs of *D* and *G* bands observed for the sample with Ni/SiC metallization. XRD and RBS profiles discussed in this work suggest a nonuniform distribution of carbon structures in metallization layer. Relatively large values of FWHM for this pair of bands suggest scattering of the structural parameters of the species responsible for the presence of pair of "broad" *D* and *G* bands.

Table 5: Electrical properties of Au/Ni_2Si/n-SiC and Au/$Ta_{35}Si_{15}N_{50}$/Ni_2Si/n-SiC ohmic contacts versus heat treatments.

Heat treatments	Au/Ni_2Si/n-SiC		Au/$Ta_{35}Si_{15}N_{50}$/Ni_2Si/n-SiC	
	r_c ($\times 10^{-4}\ \Omega\,cm^2$)	R_{sh} (Ω/sq)	r_c ($\times 10^{-4}\ \Omega\,cm^2$)	R_{sh} (Ω/sq)
As-deposited	~4	0.29	~4	0.29
800°C/Ar/3 min	~4.5	0.26	~4	0.22
400°C/air/150 h	Nonohmic	0.68	~4.5	0.17

4.6. Thermal Stability of Ni_2Si-Based Ohmic Contacts to n-Type 4H-SiC. Fabrication of low-resistive ohmic contacts to silicon carbide (SiC) is not sufficient for application to SiC-based devices. For usage of those SiC-based devices in harsh environments, investigation of their reliability, for example, thermal stability, is needed [85–92]. In order to investigate the thermal stability of Ni_2Si-based ohmic contacts to n-type 4H-SiC, the influence of heat treatment conditions, such as long-term aging in air at 400°C and rapid thermal annealing (RTA) in a neutral atmosphere (Ar) at 800°C, on the reliability of Ni_2Si/n-SiC ohmic contacts with a top Au mounting layer was studied. A part of the prepared structures had a Ta-Si-N diffusion barrier introduced between the Ni_2Si and Au layers. Gold has been chosen as the overlayer for interconnection or bonding metallization, as it is a highly conductive metal compatible with the standard semiconductor technology. The nanocomposite Ta-Si-N layers selected for the diffusion barriers were shown to have excellent diffusion-blocking properties in contacts to Si [92], GaAs [93, 94], and GaN [95].

The electrical properties before and after heat treatments of the Au (150 nm)/Ni_2Si/n-SiC and Au (150 nm)/$Ta_{35}Si_{15}N_{50}$ (100 nm)/Ni_2Si/n-SiC ohmic contact stacks are summarized in Figure 15 and Table 5. The specific contact resistance $r_c \sim 4 \times 10^{-4}\ \Omega\,cm^2$ for the as-deposited Au/Ni_2Si/n-SiC contacts remains unchanged after RTA at 800°C (Ar, 3 min); however, the I-V characteristics start to exhibit nonohmic behavior after aging at 400°C (air, 150 h). For the Au/TaSiN/Ni_2Si/n-SiC contacts, the $r_c \sim 4\times 10^{-4}\ \Omega\,cm^2$ remains unchanged after RTA at 800°C (Ar, 3 min) as well as after aging at 400°C (air, 150 h). The initial sheet resistance ($R_{sh} \sim 0.29\ \Omega$/sq) for both as-deposited contacts corresponds to the resistivity of highly conductive 150 nm thick Au overlayer ($\rho \sim 4.4\ \mu\Omega\,cm$). This value exceeds the resistivity of bulk Au ($\rho \sim 2.5\ \mu\Omega\,cm$ [96]) due to the scattering of electrons by the film grain boundaries. For the Au/Ni_2Si/n-SiC contacts, R_{sh} decreases by ~10% and increases by ~230% after RTA (800°C, Ar) and aging (400°C, air), respectively. On the contrary, for the Au/TaSiN/Ni_2Si/n-SiC contacts, R_{sh} decreases by ~25% and ~40% after RTA (800°C, Ar) and aging (400°C, air), respectively. The observed decrease in R_{sh} can be related to recrystallization of the Au layers with a subsequent reduction of grain boundary density. One of the reasons for such an explanation is the fact that $R_{sh} \sim 0.2\ \Omega$/sq for the treated contacts corresponds to the resistivity $\rho \sim 3\ \mu\Omega\,cm$ which is very close to the value for bulk Au. On the other hand, the increase of r_c and R_{sh} can be attributed to the diffusion processes in metallization systems under thermal stress. For further studies of these contacts XRD, RBS, and SEM techniques were applied.

XRD spectra of the Au/Ni_2Si/n-SiC and Au/TaSiN/Ni_2Si/n-SiC contact stacks before and after heat treatments are shown in Figure 16. The XRD spectra of the as-deposited stacks are similar in both cases. Apart from the (0004) peak of the single crystal 4H-SiC, only peaks from polycrystalline Au (111) and orthorhombic δ-Ni_2Si (013) are observed, showing that the Au and δ-Ni_2Si grains are textured. After annealing at 800°C (Ar, 3 min), for both stacks only a small shift of the Au and δ-Ni_2Si peaks to higher Bragg angles is detected due to the recrystallization of Au grains and strain relaxation at the Au/contact interface. Similar changes are observed in the XRD spectra (Figure 16(b)) for the Au/TaSiN/Ni_2Si/n-SiC stacks after aging at 400°C (air, 150 h). However, when the same aging conditions were applied to the Au/Ni_2Si/n-SiC stacks, a strong decrease in the intensity of the (013) δ-Ni_2Si peak, splitting of the (111) Au peak, and an appearance of new peaks were observed (Figure 14(a)). This can be interpreted as a decomposition of Ni_2Si leading to the formation of pure Ni and $Ni_{31}Si_{12}$ phases as well as a $Au_x(Ni{:}Si)_{1-x}$ solid solution.

RBS profiles of the Au/Ni_2Si/n-SiC contact stacks are shown in Figure 17(a). The only difference between the profiles measured for the as-deposited and RTP-annealed (800°C, Ar, 3 min) samples is the appearance of a small Ni surface signal (~1.5 MeV). Apart from this feature, the profiles overlap which indicates no redistribution of the elements after annealing. However, subsequent aging of the stacks at 400°C (air, 150 h) results in a considerable change of the RBS profiles. Significant changes of the signal from Au, the disappearance of the signal from Ni_2Si, and the appearance of Ni (~1.5 MeV) and O (~0.7 MeV) signals are observed. This indicates a strong interaction at both the Au/Ni_2Si and Ni_2Si/n-SiC interfaces after aging. Simulation shows an in-diffusion of Au atoms into the contact, out-diffusion of Ni and Si atoms to the surface, and oxygen penetration into the contact. This correlates well with the strong degradation of the electrical properties of the contacts observed (see Table 5). On the other hand, the overlap of the RBS profiles for the as-deposited, annealed at 800°C (Ar, 3 min), and aged at 400°C (air, 150 h) Au/TaSiN/Ni_2Si/n-SiC contact stacks shown in Figure 15(b) indicates that the Ta-Si-N diffusion barrier introduced between the Au overlayer and the Ni_2Si/n-SiC ohmic contact successfully blocks any interdiffusion and retains abrupt interfaces with the neighbouring layers.

Figure 18 shows SEM images of the Au/Ni_2Si/n-SiC and Au/$Ta_{35}Si_{15}N_{50}$/Ni_2Si/n-SiC contact stacks before and after heat treatments. The surface morphology of the as-deposited contacts is shown in Figures 18(a) and 18(c) and appears relatively smooth. Annealing of the Au/Ni_2Si/n-SiC stacks at 800°C (Ar, 3 min) leads to a modification of the gold

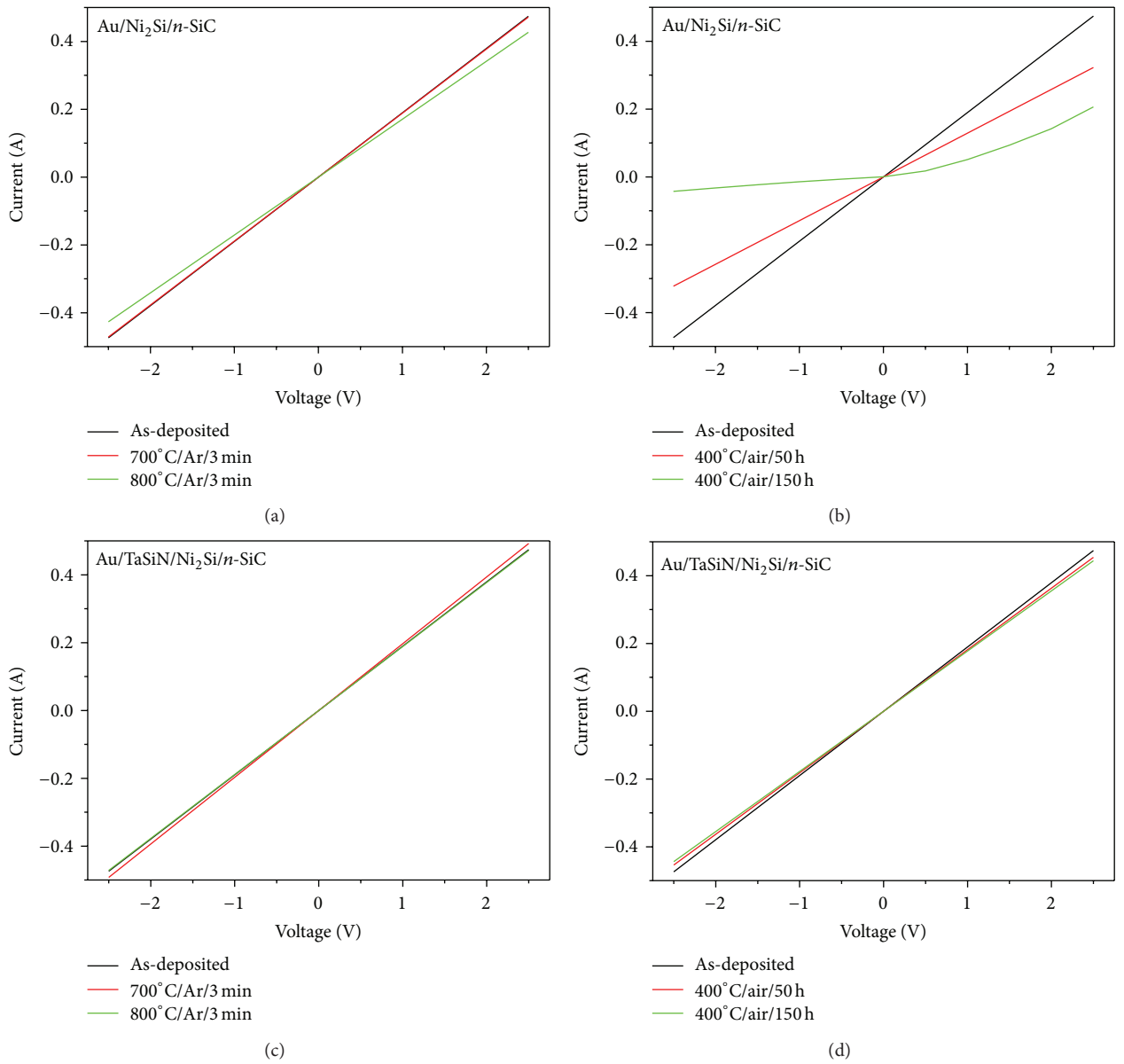

FIGURE 15: Current-voltage characteristics for the Au/Ni_2Si/*n*-SiC (a, b) and Au/$Ta_{35}Si_{15}N_{50}$/Ni_2Si/*n*-SiC (c, d) ohmic contacts versus heat treatments.

surface, due to a recrystallization leading to an increase of Au grain size and subsequent pore formation in the Au layer (Figure 16(a)). The pores are responsible for the appearance of the Ni surface signal in the RBS spectrum of this contact stack (Figure 17(a)). Similar surface changes are detected for the Au/TaSiN/Ni_2Si/*n*-SiC contact stack after annealing at 800°C (Ar, 3 min), but a smaller number of pores in the Au layer are observed (Figure 18(c)). For the Au/Ni_2Si/*n*-SiC contacts aged at 400°C (air, 150 h), granular areas and craters appear in the Au layer, both indicating strong morphology degradation (Figure 18(b)). The depth of the craters (≥295 nm) exceeds the thickness (~250 nm) of the Au/Ni_2Si metallization and their average surface density is about 2000 mm^{-2}. Thus, we can assume that oxygen diffuses into the contact preferentially via the craters created in the metallization. Aging the Au/$Ta_{35}Si_{15}N_{50}$/Ni_2Si/*n*-SiC contact stacks at 400°C (air, 150 h) results only in small modifications of the surface morphology due to the recrystallization of Au grains; the contact surface still is relatively smooth surface.

Thus, for the Au/Ni_2Si/*n*-SiC contacts without the Ta-Si-N diffusion barrier, the degradation of the electrical characteristics correlates well with phase transformation, depth redistribution of elements, and oxygen penetration. It has to be noted that it was previously reported that the degradation of electrical properties in air comes mainly from the diffusion of oxygen into the contacts [97, 98]. However, apart from the oxidation of the contacts, oxygen

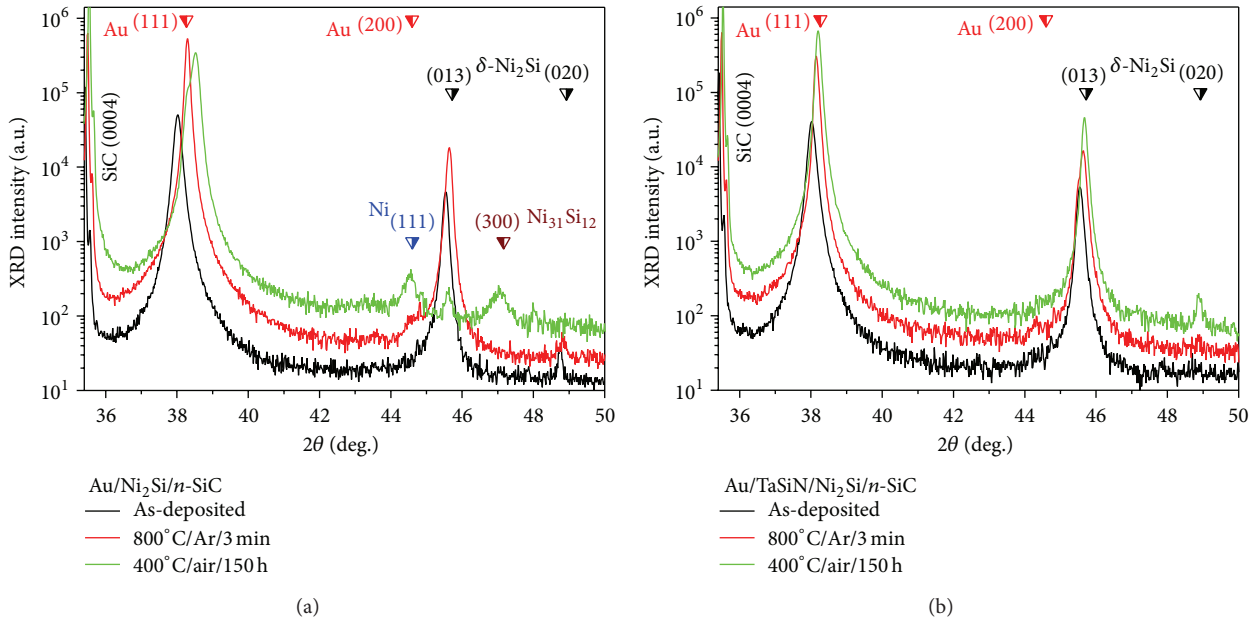

FIGURE 16: XRD spectra of the Au/Ni_2Si/n-SiC (a) and Au/$Ta_{35}Si_{15}N_{50}$/Ni_2Si/n-SiC (b) ohmic contacts before and after heat treatments.

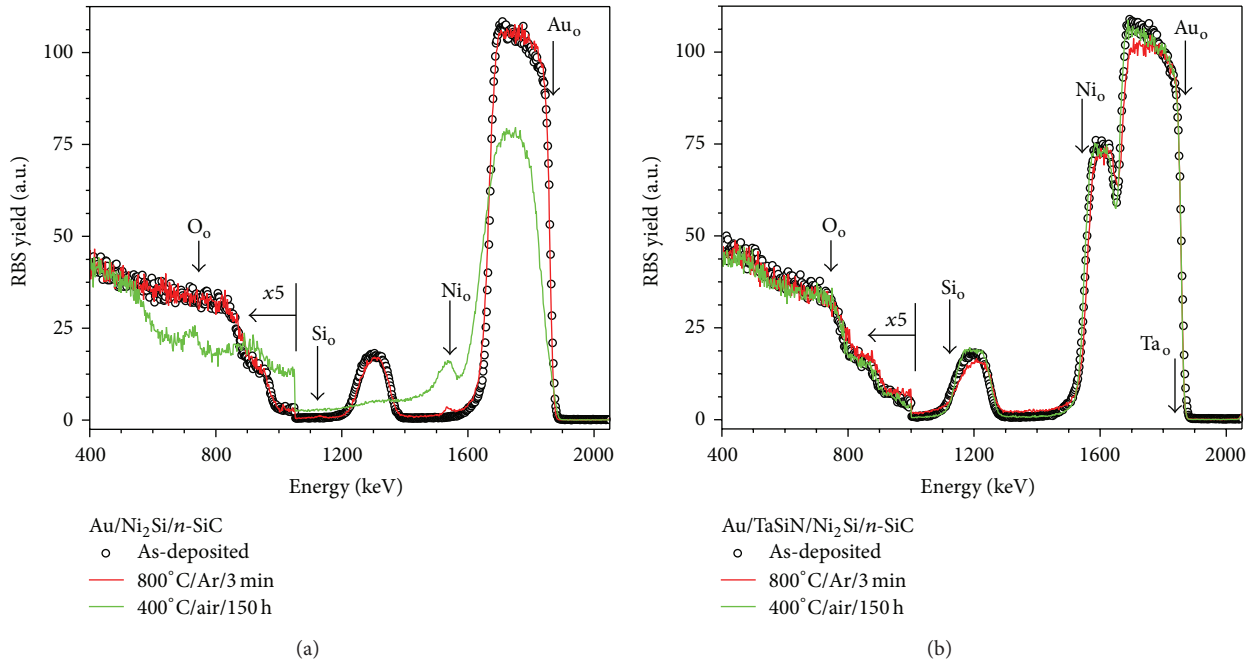

FIGURE 17: RBS spectra of the Au/Ni_2Si/n-SiC (a) and Au/$Ta_{35}Si_{15}N_{50}$/Ni_2Si/n-SiC (b) ohmic contacts before and after heat treatments. By an arrow are marked the surface energies of the respective elements.

plays the role of a catalyst, which enhances interdiffusion and/or reaction in metal/SiC contacts. Investigations of the Au/TaSiN/Ni_2Si/n-SiC contacts show their superior thermal stability. This can be concluded from the abrupt contact interfaces, no redistribution of the elements over the depth as well as from the preserved smooth surface and the phase composition after heat treatments.

We conclude that the thermal stability of Ni_2Si/n-SiC ohmic contacts with Au overlayer depends mainly on the heat treatment conditions as well as the presence of a diffusion barrier. We observed that degradation of the ohmic contacts becomes stronger after long-time aging in air at relatively low temperature (400°C) than after RTA at 800°C in a neutral gas (Ar). An optimized $Ta_{35}Si_{15}N_{50}$ diffusion barrier introduced

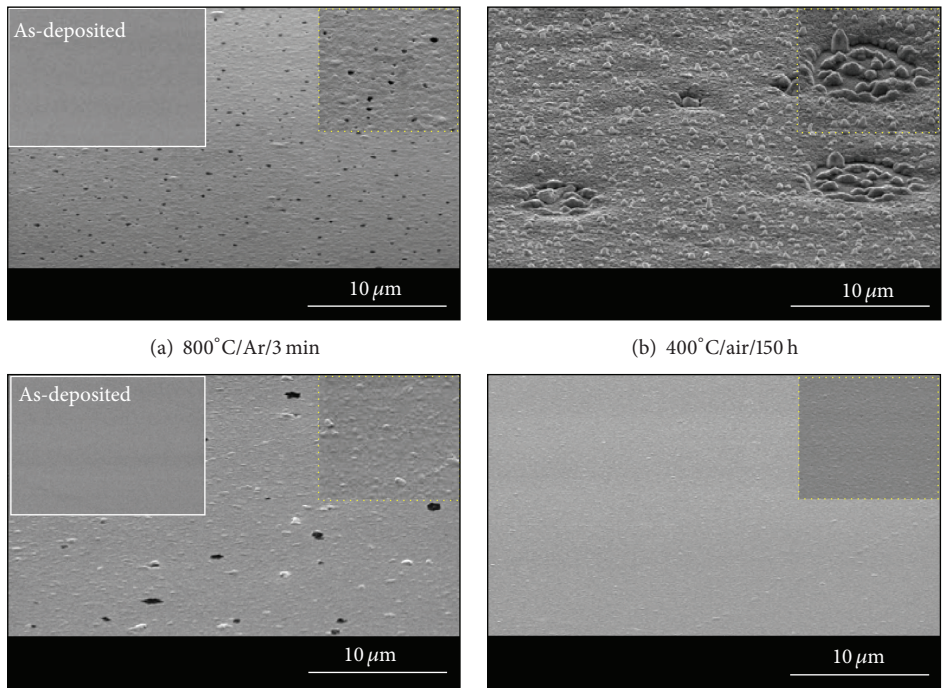

(a) 800°C/Ar/3 min (b) 400°C/air/150 h

(c) 800°C/Ar/3 min (d) 400°C/air/150 h

FIGURE 18: SEM micrographs of the Au/Ni_2Si/*n*-SiC (a and b) and Au/$Ta_{35}Si_{15}N_{50}$/Ni_2Si/*n*-SiC (c and d) ohmic contacts: (a, c) as-deposited and after annealing in Ar at 800°C (3 min); (b, d) after aging in air at 400°C (150 h) [85–88]. The yellow squares show the SEM micrographs with higher resolution for the contacts after heat treatments.

between the Ni_2Si/*n*-SiC ohmic contact and Au overlayer prevents the interdiffusion of metals in the contact region, as well as the penetration of oxygen during long-time aging in air.

5. Discussion and Conclusions

The common processes in the reaction of metals with SiC could be as follows: formation of silicides and free carbon or formation of carbides and silicides [99]. The properties of the contact materials affect the final reaction products. Concerning the Ni-based metallization, the Ni-silicides and free carbon are formed during the reaction of pure Ni with SiC. Both carbides and silicides are formed by adding a strong carbide former metal (Ti, Mo, etc.) to the Ni-based metallization scheme [13, 44, 91, 100, 101].

Many technological parameters have strong influence on Ni-based metal reaction with SiC. All these parameters can affect both the structural and electrical properties of the contacts. Nevertheless, some common features become evident: (i) the formation of the Ni_2Si phase either by an interaction between Ni and SiC, by a solid state reaction between Ni and Si single layers, or by a deposition of Ni_2Si layers on SiC creates a relatively high quality Schottky contact to *n*-SiC up to annealing ≤700°C; (ii) annealing at high temperature (>900°C) leads to the transition from rectifying to ohmic contact for the same metallization. Both Ni-based Schottky and ohmic contacts annealed at different temperature are used for SiC-based semiconductor devices [102–105]. There are many studies that show a consensus of Ni_2Si/*n*-SiC Schottky contacts which have the barrier height $\varphi_B \sim 1.6$ eV [10–12, 16–18, 29–32]. However, there is still little consensus regarding why the barrier height decreases and Ni_2Si/*n*-SiC contacts become ohmic after annealing at temperature or above 900°C. How does the Ni_2Si phase create both Schottky and ohmic contacts to *n*-SiC?

A steep reduction of specific contact resistances and decrease in φ_B at temperatures over 900°C for Ni-based ohmic contact to *n*-SiC was observed by Tanimoto et al. [106]. Using cross-sectional TEM-EDS (energy dispersive X-ray spectroscopy) analysis has made such conclusions: (i) the surface of substrates annealed at 1000°C was not covered with Ni_2Si but with a thin layer of NiSi; (ii) the formation of the NiSi/SiC system contributes to the significant reduction in contact resistance. On the other hand, in the series of papers particular attention was paid to the role of carbon placed on the silicide/SiC interface [77, 107, 108]. It was shown that carbon on this interface can play catalytic role in the formation of ohmic contact. The transition from Schottky to ohmic behavior was achieved after annealing in 800°C. This temperature is significantly lower in comparison with standard values reported for samples without additional carbon layer deposited on the interface during the manufacturing process. Ni-silicides appear generally at temperatures between 400 and 600°C [50, 109]. The hypothesis that the graphite layer placed on the interface is responsible for the ohmic character of contact was supported by ohmic character of graphite layer placed on silicon carbide [51]. However, as

was shown, the carbon atoms can be present on the interface at the temperatures in which ohmic character of the contact is not observed. On the other side, the diffusion of carbon atoms towards the free silicide surface was observed at higher temperatures than the temperature necessary for creation of a silicide layer [54]. The other postulated mechanism responsible for ohmic character of the contact is related to structural changes of the SiC substrate in close vicinity of silicide/SiC interface [110]. These changes are caused by creation of empty places, so-called vacancies, which lower the Schottky barrier [42, 71, 111]. The mechanism which is suspected for creation of these vacancies is diffusion of carbon atoms towards free silicide surface [71, 111]. Moreover, using DLTS in an effort to detect a high concentration of carbon vacancies for 950°C annealed contacts suggests that this model is correct [31, 53]. All available data does not allow authors to point to one simple mechanism which can describe the contribution of carbon atoms to creation of ohmic contacts. The investigation of the samples with additional carbon layer deposited on the interface suggests only a catalytic role of this element in creation of ohmic contacts. Moreover, the data obtained in this work do not confirm the presence of carbon atoms on the Ni_2Si/SiC interface. This suggests that contribution of carbon to ohmic contact creation may be very complex and the exact mechanism may be modified by parameters of the whole manufacturing process.

Thus, based on our reported results, we may conclude that only δ-Ni_2Si grains play a key role in determining electrical transport properties at the contact/SiC interface. It should be noted that the creation of Ni_2Si phase on *n*-SiC is not sufficient for the formation of an ohmic contact. Only the recrystallization of Ni_2Si phase after annealing at high temperature (>900°C) leads to the transition from rectifying to ohmic contact by lowering barrier height from ~1.6 eV to ~0.45 eV. We suppose that only δ-Ni_2Si grains that are in the orientation-relationship with (0001)SiC//(013) δ-Ni_2Si after high-temperature annealing are area with low barrier height [71]. Indeed, from Ni-silicides only δ-Ni_2Si is thermodynamically stable with SiC, which agrees well with the Ni-Si-C ternary phase diagram (tie lines connect δ-Ni_2Si with SiC and C) [112].

Vivona et al. [113] demonstrated the thermal stability of the Ni_2Si/*n*-SiC ohmic contact after long-term (up to 95 h) thermal cycling in N_2 atmosphere at different temperatures (in the range 200–400°C). The thermal stability of the current transport mechanisms, the specific contact resistance, and barrier height (~0.45 eV) were observed. At the same time, annealing in air [85–88] leads to the catastrophic degradation of omicity of the Ni_2Si/*n*-SiC contact. Thus, the diffusion barriers with free diffusion path microstructure are key elements to improve thermal stability of metal-SiC ohmic contacts for high-temperature electronics.

Finally, summarizing this paper, we conclude that manufacturing of high quality ohmic contacts requires optimization of "multiparametric function." The parameters that should be included are (i) quality of silicon carbide; (ii) surface before treatment; (iii) metallization scheme (type of metals, thicknesses, sequence of deposition, and diffusion barrier); (iv) contact passivation against corrosion; and (v) annealing type (sequence of temperature and application time, atmosphere of thermal process, and cooling and heating ratios).

Competing Interests

The authors declare that there are no competing interests regarding the publication of this paper.

Acknowledgments

The authors wish to thank Dr. R. Minikayev (Institute of Physics, Warsaw, Poland), Dr. O. Lytvyn (V. Lashkaryov Institute of Semiconductor Physics, Kyiv, Ukraine), and M. Latek (Institute of Electron Technology, Warsaw, Poland)/Dr. O. Kolomys (V. Lashkaryov Institute of Semiconductor Physics, Kyiv, Ukraine) for XRD, AFM, and Raman measurements, respectively.

References

[1] http://www.ioffe.ru/SVA/NSM/.

[2] T. Kimoto and J. A. Cooper, *Fundamentals of Silicon Carbide Technology: Growth, Characterization, Devices, and Applications*, John Wiley & Sons, Singapore, 2014.

[3] P. Friedrichs, T. Kimoto, L. Ley, and G. Pensl, *Silicon Carbide: Growth, Defects, and Novel Applications*, vol. 1, Wiley-VCH Verlag GmbH & Co. KGaA, Weinheim, Germany, 2010.

[4] L. M. Porter and R. F. Davis, "A critical review of ohmic and rectifying contacts for silicon carbide," *Materials Science and Engineering B*, vol. 34, no. 2-3, pp. 83–105, 1995.

[5] J. Crofton, L. M. Porter, and J. R. Williams, "The physics of Ohmic contacts to SiC," *Physica Status Solidi (B): Basic Research*, vol. 202, no. 1, pp. 581–603, 1997.

[6] F. Roccaforte, F. La Via, and V. Raineri, "Ohmic contacts to SiC," *International Journal of High Speed Electronics and Systems*, vol. 15, no. 4, pp. 781–820, 2005.

[7] W. R. Harrell, J. Zhang, and K. F. Poole, "Aluminum Schottky contacts to n-type 4H-SiC," *Journal of Electronic Materials*, vol. 31, no. 10, pp. 1090–1095, 2002.

[8] U. Zimmermann, A. Hallen, and B. Breitholtz, "Current voltage characteristics of high-voltage 4H silicon carbide diodes," *Materials Science Forum*, vol. 338–342, pp. 1323–1326, 2000.

[9] K. P. Schoen, J. M. Woodall, J. A. Cooper, and M. R. Melloch, "Design considerations and experimental analysis of high-voltage SiC Schottky barrier rectifiers," *IEEE Transactions on Electron Devices*, vol. 45, no. 7, pp. 1595–1604, 1998.

[10] A. Itoh and H. Matsunami, "Analysis of schottky barrier heights of metal/SiC contacts and its possible application to high-voltage rectifying devices," *Physica Status Solidi (A)*, vol. 162, no. 1, pp. 389–408, 1997.

[11] D. Perrone, M. Naretto, S. Ferrero, L. Scaltrito, and C. F. Pirri, "4H-SiC schottky barrier diodes using Mo-, Ti- and Ni-based contacts," *Materials Science Forum*, vol. 615–617, pp. 647–650, 2009.

[12] F. La Via, F. Roccaforte, A. Makhtari, V. Raineri, P. Musumeci, and L. Calcagno, "Structural and electrical characterisation of titanium and nickel silicide contacts on silicon carbide," *Microelectronic Engineering*, vol. 60, no. 1-2, pp. 269–282, 2002.

[13] P. A. Ivanov, A. S. Potapov, and T. P. Samsonova, "Analysis of forward current-voltage characteristics of non-ideal Ti/$_4$H-SiC Schottky barriers," *Materials Science Forum*, vol. 615–617, pp. 431–434, 2009.

[14] T. Hatayama, K. Kawahito, H. Kijima, Y. Uraoka, and T. Fuyuki, "Electrical properties and interface reaction of annealed Cu/4H-SiC schottky rectifiers," *Materials Science Forum*, vol. 389–393, pp. 925–928, 2002.

[15] C. Koliakoudakis, J. Dontas, S. Karakalos et al., "Fabrication and characterization of Cr-based Schottky Diode on n-type 4H-SiC," *Materials Science Forum*, vol. 615–617, pp. 651–654, 2009.

[16] A. Kestle, S. P. Wilks, P. R. Dunstan, M. Pritchard, and P. A. Mawby, "Improved Ni/SiC Schottky diode formation," *Electronics Letters*, vol. 36, no. 3, pp. 267–268, 2000.

[17] V. Saxena, J.-N. Su, and A. J. Steckl, "High-voltage Ni- and Pt-SiC Schottky diodes utilizing metal field plate termination," *IEEE Transactions on Electron Devices*, vol. 46, no. 3, pp. 456–464, 1999.

[18] I. Nikitina, K. Vassilevski, A. Horsfall et al., "Phase inhomogeneity and electrical characteristics of nickel silicide Schottky contacts formed on 4H-SiC," *Materials Science Forum*, vol. 615–17, pp. 577–580, 2009.

[19] W. Jung and M. Guziewicz, "Schottky diode parameters extraction using Lambert W function," *Materials Science and Engineering: B*, vol. 165, no. 1-2, pp. 57–59, 2009.

[20] H.-J. Im, B. Kaczer, J. P. Pelz, and W. J. Choyke, "Ballistic electron emission microscopy study of Schottky contacts on 6*H*- and 4*H*-SiC," *Applied Physics Letters*, vol. 72, no. 7, pp. 839–841, 1998.

[21] H.-J. Im, B. Kaczer, J. P. Pelz, J.-M. Chen et al., "Nanometer-scale investigation of Schottky contacts and conduction band structure on 4*H*-, 6*H*- and 15*R*-SiC using ballistic electron emission microscopy," *Materials Science Forum*, vol. 264–268, pp. 813–816, 1998.

[22] O. Shigiltchoff, T. Kimoto, D. Hoodgood et al., "Schottky barriers for Pt, Mo and Ti on 6H and 4H SiC (0001), (0001), (1100) and (1210) faces measured by I-V, C-V and internal photoemission," in *Proceedings of the Technical Digest of International Conference on SiC and Related Materials We-B-23*, p. 291, Tsukuba, Japan, 2001.

[23] A. F. Hamida, Z. Ouennoughi, A. Sellai, R. Weiss, and H. Ryssel, "Barrier inhomogeneities of tungsten Schottky diodes on 4H-SiC," *Semiconductor Science and Technology*, vol. 23, no. 4, Article ID 045005, 2008.

[24] C. F. Zhe, *Silicon Carbide: Materials, Processing & Devices*, Taylor & Francis, New York, NY, USA, 2004.

[25] M. Wiets, M. Weinelt, and T. Fauster, "Electronic structure of SiC(0001) surfaces studied by two-photon photoemission," *Physical Review B*, vol. 68, no. 12, Article ID 125321, 2003.

[26] A. V. Kuchuk, V. P. Kladko, M. Guziewicz et al., "Fabrication and characterization of nickel silicide ohmic contacts to n-type 4H silicon carbide," *Journal of Physics: Conference Series*, vol. 100, part 4, Article ID 042003, 2008.

[27] J. Crofton, P. G. McMullin, J. R. Williams, and M. J. Bozack, "High−temperature ohmic contact to *n*−type 6H−SiC using nickel," *Journal of Applied Physics*, vol. 77, no. 3, pp. 1317–1319, 1995.

[28] M. G. Rastegaeva, A. N. Andreev, A. A. Petrov, A. I. Babanin, M. A. Yagovkina, and I. P. Nikitina, "The influence of temperature treatment on the formation of Ni-based Schottky diodes and ohmic contacts to n-6H-SiC," *Materials Science and Engineering B*, vol. 46, no. 1–3, pp. 254–258, 1997.

[29] S. P. Avdeev, O. A. Agueev, R. V. Konakova et al., "Effect of pulse thermal treatments on the Ni(Ti)/n-21R(6H)-SiC contact parameters," *Semiconductor Physics, Quantum Electronics & Optoelectronics*, vol. 7, no. 3, pp. 272–278, 2004.

[30] T. Marinova, V. Krastev, C. Hallin, R. Yakimova, and E. Janzén, "Interface chemistry and electric characterisation of nickel metallisation on 6H-SiC," *Applied Surface Science*, vol. 99, no. 2, pp. 119–125, 1996.

[31] F. La Via, F. Roccaforte, V. Raineri et al., "Schottky-ohmic transition in nickel silicide/SiC-4H system: is it really a solved problem?" *Microelectronic Engineering*, vol. 70, no. 2–4, pp. 519–523, 2003.

[32] F. Roccaforte, F. La Via, V. Raineri, L. Calcagno, and P. Musumeci, "Improvement of high temperature stability of nickel contacts on n-type 6H-SiC," *Applied Surface Science*, vol. 184, no. 1–4, pp. 295–298, 2001.

[33] T. Marinova, A. Kakanakova-Georgieva, V. Krastev et al., "Nickel based ohmic contacts on SiC," *Materials Science and Engineering: B*, vol. 46, no. 1–3, pp. 223–226, 1997.

[34] A. Kakanakova-Georgieva, T. Marinova, O. Noblanc, C. Arnodo, S. Cassette, and C. Brylinski, "Characterization of ohmic and Schottky contacts on SiC," *Thin Solid Films*, vol. 343-344, no. 1-2, pp. 637–641, 1999.

[35] S. J. Yang, C. K. Kim, I. H. Noh, S. W. Jang, K. H. Jung, and N. I. Cho, "Study of Co- and Ni-based ohmic contacts to n-type 4H-SiC," *Diamond and Related Materials*, vol. 13, no. 4–8, pp. 1149–1153, 2004.

[36] T. Nakamura and M. Satoh, "Schottky barrier height of a new ohmic contact $NiSi_2$ to n-type 6H-SiC," *Solid-State Electronics*, vol. 46, no. 12, pp. 2063–2067, 2002.

[37] C. Deeb and A. H. Heuer, "A low-temperature route to thermodynamically stable ohmic contacts to *n*-type 6H-SiC," *Applied Physics Letters*, vol. 84, no. 7, p. 1117, 2004.

[38] A. V. Kuchuk, V. P. Kladko, A. Piotrowska, R. Ratajczak, and R. Jakiela, "On the formation of Ni-based ohmic contacts to n-type 4H-SiC," *Materials Science Forum*, vol. 615–617, pp. 573–576, 2009.

[39] E. Kurimoto, H. Harima, T. Toda, M. Sawada, M. Iwami, and S. Nakashima, "Raman study on the Ni/SiC interface reaction," *Journal of Applied Physics*, vol. 91, no. 12, pp. 10215–10217, 2002.

[40] T. Seyller, K. V. Emtsev, K. Gao et al., "Structural and electronic properties of graphite layers grown on SiC(0 0 0 1)," *Surface Science*, vol. 600, no. 18, pp. 3906–3911, 2006.

[41] L. Calcagno, A. Ruggiero, F. Roccaforte, and F. La Via, "Effects of annealing temperature on the degree of inhomogeneity of nickel-silicide/SiC Schottky barrier," *Journal of Applied Physics*, vol. 98, no. 2, Article ID 023713, 2005.

[42] I. P. Nikitina, K. V. Vassilevski, N. G. Wright, A. B. Horsfall, A. G. O'Neill, and C. M. Johnson, "Formation and role of graphite and nickel silicide in nickel based ohmic contacts to n-type silicon carbide," *Journal of Applied Physics*, vol. 97, no. 8, Article ID 083709, 2005.

[43] W. Lu, W. C. Mitchel, G. R. Landis, T. R. Crenshaw, and W. E. Collins, "Catalytic graphitization and Ohmic contact formation on 4H-SiC," *Journal of Applied Physics*, vol. 93, no. 9, pp. 5397–5403, 2003.

[44] M. H. Ervin, K. A. Jones, M. A. Derenge et al., "In situ SEM observations and electrical measurements during the annealing of Si/Ni contacts to SiC," in *Proceedings of the Materials Research Society Symposium*, vol. 764 of *MRS Proceeding*, 2003.

[45] B. Barda, P. Machac, M. Hubickova, and J. Nalik, "Comparison of Ni/Ti and Ni ohmic contacts on *n*-type 6H–SiC," *Journal of Materials Science: Materials in Electronics*, vol. 19, no. 11, pp. 1039–1044, 2008.

[46] G. V. Samsonov and I. M. Vinitdky, *Refractory Compounds*, Metallurgija, Moscow, Russia, 1976 (Russian).

[47] L. J. Chen, *Silicide Technology for Integrated Circuits (Processing)*, Institution of Electrical Engineers, 2004.

[48] N. Biswas, J. Gurganus, and V. Misra, "Work function tuning of nickel silicide by co-sputtering nickel and silicon," *Applied Physics Letters*, vol. 87, no. 17, Article ID 171908, 2005.

[49] A. Bächli, M.-A. Nicolet, L. Baud, C. Jaussaud, and R. Madar, "Nickel film on (001) SiC: thermally induced reactions," *Materials Science and Engineering: B*, vol. 56, no. 1, pp. 11–23, 1998.

[50] Z. Zhang, J. Teng, W. X. Yuan, F. F. Zhang, and G. H. Chen, "Kinetic study of interfacial solid state reactions in the Ni/4H–SiC contact," *Applied Surface Science*, vol. 255, no. 15, pp. 6939–6944, 2009.

[51] W. Lu, W. C. Mitchel, C. A. Thornton, G. R. Landis, and W. Eugene Collins, "Carbon structural transitions and ohmic contacts on 4H–SiC," *Journal of Electronic Materials*, vol. 32, no. 5, pp. 426–431, 2003.

[52] S. Y. Han and J.-L. Lee, "Effect of interfacial reactions on electrical properties of Ni contacts on lightly doped n-type 4H–SiC," *Journal of the Electrochemical Society*, vol. 149, no. 3, pp. G189–G193, 2002.

[53] L. Calcagno, E. Zanetti, F. La Via et al., "Schottky-ohmic transition in nickel sllicide/SiC system: is it really a solved problem?" *Materials Science Forum*, vol. 433–436, pp. 721–724, 2003.

[54] R. Colby, M. L. Bolen, M. A. Capano, and E. A. Stach, "Amorphous interface layer in thin graphite films grown on the carbon face of SiC," *Applied Physics Letters*, vol. 99, no. 10, Article ID 101904, 2011.

[55] A. Hähnel, V. Ischenko, and J. Woltersdorf, "Oriented growth of silicide and carbon in SiC-based sandwich structures with nickel," *Materials Chemistry and Physics*, vol. 110, no. 2-3, pp. 303–310, 2008.

[56] A. Hähnel, E. Pippel, V. Ischenko, and J. Woltersdorf, "Nanostructuring in Ni/SiC reaction layers, investigated by imaging of atomic columns and DFT calculations," *Materials Chemistry and Physics*, vol. 114, no. 2-3, pp. 802–808, 2009.

[57] A. A. Woodworth and C. D. Stinespring, "Surface chemistry of Ni induced graphite formation on the 6H-SiC (0 0 0 1) surface and its implications for graphene synthesis," *Carbon*, vol. 48, no. 7, pp. 1999–2003, 2010.

[58] J. C. Burton, L. Sun, F. H. Long, Z. C. Feng, and I. T. Ferguson, "First- and second-order Raman scattering from semi-insulating 4H-SiC," *Physical Review B—Condensed Matter and Materials Physics*, vol. 59, no. 11, pp. 7282–7284, 1999.

[59] P. Borowicz, A. Kuchuk, Z. Adamus et al., "Structure of carbonic layer in ohmic contacts: comparison of silicon carbide/carbon and carbon/silicide interfaces," *ISRN Physical Chemistry*, vol. 2013, Article ID 487485, 11 pages, 2013.

[60] M. Mayer, "SIMNRA, a simulation program for the analysis of NRA, RBS and ERDA," in *Proceedings of the 15th International Conference on the Application of Accelerators in Research and Industry*, J. L. Duggan and I. L. Morgan, Eds., vol. 475, p. 541, 1999, AIP Conference Proceedings.

[61] B. Pécz, G. Radnóczi, S. Cassette, C. Brylinski, C. Arnodo, and O. Noblanc, "TEM study of Ni and Ni_2Si ohmic contacts to SiC," *Diamond and Related Materials*, vol. 6, no. 10, pp. 1428–1431, 1997.

[62] M. W. Cole, P. C. Joshi, and M. Ervin, "Fabrication and characterization of pulse laser deposited Ni_2Si Ohmic contacts on *n*-SiC for high power and high temperature device applications," *Journal of Applied Physics*, vol. 89, no. 8, pp. 4413–4416, 2001.

[63] I. Nikitina, K. Vassilevski, A. Horsfall et al., "Phase composition and electrical characteristics of nickel silicide Schottky contacts formed on 4H–SiC," *Semiconductor Science and Technology*, vol. 24, no. 5, Article ID 055006, 2009.

[64] G. Hui, Z. Yi-Men, Q. Da-Yong, S. Lei, and Z. Yu-Ming, "The fabrication of nickel silicide ohmic contacts to n-type 6H-silicon carbide," *Chinese Physics*, vol. 16, no. 6, pp. 1753–1756, 2007.

[65] P. Colombi, E. Bontempi, U. M. Meotto et al., "Amorphous Ni–Zr layer applied for microstructure improvement of Ni-based ohmic contacts to SiC," *Materials Science and Engineering B*, vol. 114-115, pp. 236–240, 2004.

[66] A. V. Kuchuk, K. Gołaszewska, V. P. Kladko et al., "The formation mechanism of Ni-based ohmic contacts to 4H-n-SiC," *Materials Science Forum*, vol. 717–720, pp. 833–836, 2012.

[67] M. Wzorek, A. Czerwinski, A. Kuchuk, J. Ratajczak, A. Piotrowska, and J. Katcki, "TEM characterisation of suicide phase formation in Ni-based ohmic contacts to 4H n-SiC," *Materials Transactions*, vol. 52, no. 3, pp. 315–318, 2011.

[68] M. Wzorek, A. Czerwinski, A. Kuchuk, J. Ratajczak, A. Piotrowska, and J. Kątcki, "Ni-based ohmic contacts to silicon carbide examined by electron microscopy," *Solid State Phenomena*, vol. 186, pp. 82–85, 2012.

[69] M. Wzorek, A. Czerwinski, M. A. Borysiewicz et al., "Amorphous Ni–Zr layer applied for microstructure improvement of Ni-based ohmic contacts to SiC," *Materials Science and Engineering: B*, vol. 199, pp. 42–47, 2015.

[70] M. Wzorek, A. Czerwinski, J. Ratajczak et al., "Microstructure characterization of Si/Ni contact layers on *n*-type 4H-SiC by TEM and XEDS," *Materials Science Forum*, vol. 778–780, pp. 697–701, 2014.

[71] S. Y. Man, K. H. Kim, J. K. Kim et al., "Ohmic contact formation mechanism of Ni on n-type 4H–SiC," *Applied Physics Letters*, vol. 79, no. 12, pp. 1816–1818, 2001.

[72] A. Y. C. Yu, "Electron tunneling and contact resistance of metal-silicon contact barriers," *Solid-State Electronics*, vol. 13, no. 2, pp. 239–247, 1970.

[73] K. Ito, T. Onishi, H. Takeda et al., "Simultaneous formation of Ni/Al ohmic contacts to both n- and p-type 4H-SiC," *Journal of Electronic Materials*, vol. 37, no. 11, pp. 1674–1680, 2008.

[74] Electronic Archive, New Semiconductor Materials, Characteristics and Properties, http://www.ioffe.ru/SVA/NSM/Semicond/SiC/bandstr.html.

[75] M. Y. Zaman, D. Perrone, S. Ferrero, L. Scaltrito, and M. Naretto, "Evaluation of correct value of Richardson's constant by analyzing the electrical behavior of three different diodes at different temperatures," *Materials Science Forum*, vol. 711, pp. 174–178, 2012.

[76] S. A. Reshanov, K. V. Emtsev, F. Speck et al., "Effect of an intermediate graphite layer on the electronic properties of metal/SiC contacts," *Physica Status Solidi B: Basic Research*, vol. 245, no. 7, pp. 1369–1377, 2008.

[77] W. Lu, W. C. Mitchel, G. R. Landis, T. R. Crenshaw, and W. E. Collins, "Catalytic graphitization and Ohmic contact formation on 4H–SiC," *Journal of Applied Physics*, vol. 93, no. 9, pp. 5397–5403, 2003.

[78] A. C. Ferrari and J. Robertson, "Interpretation of Raman spectra of disordered and amorphous carbon," *Physical Review B—Condensed Matter and Materials Physics*, vol. 61, no. 20, pp. 14095–14107, 2000.

[79] A. C. Ferrari and J. Robertson, "Raman spectroscopy of amorphous, nanostructured, diamond-like carbon, and nanodiamond," *Philosophical Transactions of the Royal Society A: Mathematical, Physical and Engineering Sciences*, vol. 362, no. 1824, pp. 2477–2512, 2004.

[80] A. C. Ferrari, J. C. Meyer, V. Scardaci et al., "Raman spectrum of graphene and graphene layers," *Physical Review Letters*, vol. 97, no. 18, Article ID 187401, 2006.

[81] C. H. Lui, Z. Li, Z. Chen, P. V. Klimov, L. E. Brus, and T. F. Heinz, "Imaging stacking order in few-layer graphene," *Nano Letters*, vol. 11, no. 1, pp. 164–169, 2011.

[82] W. Norimatsu and M. Kusunoki, "Selective formation of ABC-stacked graphene layers on SiC(0001)," *Physical Review B*, vol. 81, no. 16, Article ID 161410, 2010.

[83] A. C. Ferrari, "Raman spectroscopy of graphene and graphite: disorder, electron-phonon coupling, doping and nonadiabatic effects," *Solid State Communications*, vol. 143, no. 1-2, pp. 47–57, 2007.

[84] R. Li, Z. Guo, J. Yang, X. Zeng, and W. Yuan, "Investigation of Ta/Ni bilayered ohmic contacts on n-type SiC single-crystal substrate," *Monatshefte für Chemie*, vol. 143, no. 9, pp. 1329–1334, 2012.

[85] A. V. Kuchuk, M. Guziewicz, R. Ratajczak, M. Wzorek, V. P. Kladko, and A. Piotrowska, "Long-term stability of Ni-silicide ohmic contact to n-type 4H-SiC," *Microelectronic Engineering*, vol. 85, no. 10, pp. 2142–2145, 2008.

[86] A. V. Kuchuk, M. Guziewicz, R. Ratajczak, M. Wzorek, V. P. Kladko, and A. Piotrowska, "Thermal degradation of Au/Ni_2Si/n-SiC ohmic contacts under different conditions," *Materials Science and Engineering: B*, vol. 165, no. 1-2, pp. 38–41, 2009.

[87] A. V. Kuchuk, M. Guziewicz, R. Ratajczak, M. Wzorek, V. P. Kladko, and A. Piotrowska, "Reliability tests of Au-metallized Ni-based ohmic contacts to 4H-n-SiC with and without nanocomposite diffusion barriers," *Materials Science Forum*, vol. 645–648, pp. 737–740, 2010.

[88] M. A. Borysiewicz, E. Kamińska, M. Myśliwiec et al., "Fundamentals and practice of metal contacts to wide band gap semiconductor devices," *Crystal Research and Technology*, vol. 47, no. 3, pp. 261–272, 2012.

[89] S. Liu, Z. He, L. Zheng et al., "The thermal stability study and improvement of 4H-SiC ohmic contact," *Applied Physics Letters*, vol. 105, no. 12, Article ID 122106, 2014.

[90] B. Barda, P. Macháč, S. Cichoň, and M. Kudrnová, "Thermal degradation of Ni-based Schottky contacts on 6H–SiC," *Applied Surface Science*, vol. 257, no. 9, pp. 4418–4421, 2011.

[91] C. Yue, Z. Gao-Jie, L. Yi-Hong, S. Yu-Jun, W. Tao, and C. Zhi-Zhan, "Effect of the annealing temperature on the long-term thermal stability of Pt/Si/Ta/Ti/4H–SiC contacts," *Chinese Physics B*, vol. 24, no. 10, Article ID 107303, 2015.

[92] D. P. Hamilton, M. R. Jennings, C. A. Fisher, Y. K. Sharma, S. J. York, and P. A. Mawby, "Characteristics and aging of SiC MOSFETs operated at very high temperatures," *MRS Proceedings*, vol. 1693, 2014.

[93] A. V. Kuchuk, J. Ciosek, A. Piotrowska et al., "Barrier properties of Ta-Si-N films in Ag-and Au-containing metallization," *Vacuum*, vol. 74, no. 2, pp. 195–199, 2004.

[94] A. V. Kuchuk, E. Kaminska, A. Piotrowska et al., "Amorphous Ta–Si–N diffusion barriers on GaAs," *Thin Solid Films*, vol. 459, no. 1-2, pp. 292–296, 2004.

[95] A. V. Kuchuk, V. P. Klad'ko, V. F. Machulin, and A. Piotrowska, "Thermal stability of thin amorphous Ta-Si-N films used in Au/GaN metallization," *Technical Physics*, vol. 51, no. 10, pp. 1383–1385, 2006.

[96] R. A. Serway, *Principles of Physics*, Saunders College Publishing, Fort Worth, Tex, USA, 2nd edition, 1998.

[97] M. W. Cole, P. C. Joshi, C. Hubbard, J. D. Demaree, and M. Ervin, "Thermal stability and performance reliability of Pt/Ti/WSi/Ni ohmic contacts to n-SiC for high temperature and pulsed power device applications," *Journal of Applied Physics*, vol. 91, no. 6, pp. 3864–3868, 2002.

[98] A. Virshup, L. M. Porter, D. Lukco, K. Buchholt, L. Hultman, and A. L. Spetz, "Investigation of thermal stability and degradation mechanisms in Ni-based ohmic contacts to n-type SiC for high-temperature gas sensors," *Journal of Electronic Materials*, vol. 38, no. 4, pp. 569–573, 2009.

[99] J. S. Park, K. Landry, and J. H. Perepezko, "Kinetic control of silicon carbide/metal reactions," *Materials Science and Engineering A*, vol. 259, no. 2, pp. 279–286, 1999.

[100] L. Han, H. Shen, K. Liu et al., "Improved adhesion and interface ohmic contact on n-type 4H-SiC substrate by using Ni/Ti/Ni," *Journal of Semiconductors*, vol. 35, no. 7, Article ID 072003, 2014.

[101] M. Xu, X. Hu, Y. Peng et al., "Fabrication of ohmic contact on the carbon-terminated surface of n-type silicon carbide," *Journal of Alloys and Compounds*, vol. 550, pp. 46–49, 2013.

[102] D. M. Fleetwood, E. X. Zhang, X. Shen, C. X. Zhang, R. D. Schrimpf, and S. T. Pantelides, "Bias-temperature instabilities in silicon carbide MOS devices," in *Bias Temperature Instability for Devices and Circuits*, pp. 661–675, Springer, New York, NY, USA, 2014.

[103] G. Adamo, A. Tomasino, A. Parisi et al., "Electrooptical characterization of new classes of silicon carbide UV photodetectors," *IEEE Photonics Journal*, vol. 6, no. 6, Article ID 0600707, 2014.

[104] D. Prasai, W. John, L. Weixelbaum et al., "Highly reliable silicon carbide photodiodes for visible-blind ultraviolet detector applications," *Journal of Materials Research*, vol. 28, no. 1, pp. 33–37, 2013.

[105] R. Chand, M. Esashi, and S. Tanaka, "P-N junction and metal contact reliability of SiC diode in high temperature (873 K) environment," *Solid-State Electronics*, vol. 94, pp. 82–85, 2014.

[106] S. Tanimoto, M. Miyabe, T. Shiiyama et al., "Toward a better understanding of Ni-based ohmic contacts on SiC," *Materials Science Forum*, vol. 679–680, pp. 465–468, 2011.

[107] P. Borowicz, A. Kuchuk, Z. Adamus et al., "Visible and deep-ultraviolet Raman spectroscopy as a tool for investigation of structural changes and redistribution of carbon in Ni-based Ohmic contacts on silicon carbide," *ISRN Nanomaterials*, vol. 2012, Article ID 852405, 11 pages, 2012.

[108] A. Kuchuk, V. Kladko, Z. Adamus et al., "Influence of carbon layer on the properties of Ni-based ohmic contact to n-type 4H-SiC," *ISRN Electronics*, vol. 2013, Article ID 271658, 5 pages, 2013.

[109] A. Bächli, M.-A. Nicolet, L. Baud, C. Jaussaud, and R. Madar, "Nickel film on (001) SiC: thermally induced reactions," *Materials Science and Engineering B*, vol. 56, no. 1, pp. 11–23, 1998.

[110] S. Cichoň, P. Macháč, B. Barda, and M. Kudrnová, "Si ohmic contacts on N-type SiC studied by XPS," *Microelectronic Engineering*, vol. 106, pp. 132–138, 2013.

[111] F. A. Mohammad, Y. Cao, and L. M. Porter, "Ohmic contacts to silicon carbide determined by changes in the surface," *Applied Physics Letters*, vol. 87, no. 16, Article ID 161908, pp. 1–3, 2005.

[112] Y. M. Basin, V. M. Kuznetsov, V. T. Markov, and L. S. Guzei, "Phase-equlibria in the Ni-Si-C system," *Russian Metallurgy*, vol. 4, pp. 197–200, 1988.

[113] M. Vivona, G. Greco, F. Giannazzo et al., "Thermal stability of the current transport mechanisms in Ni-based Ohmic contacts on n- and p-implanted 4H-SiC," *Semiconductor Science and Technology*, vol. 29, no. 7, Article ID 075018, 2014.